



IAEA

International Atomic Energy Agency

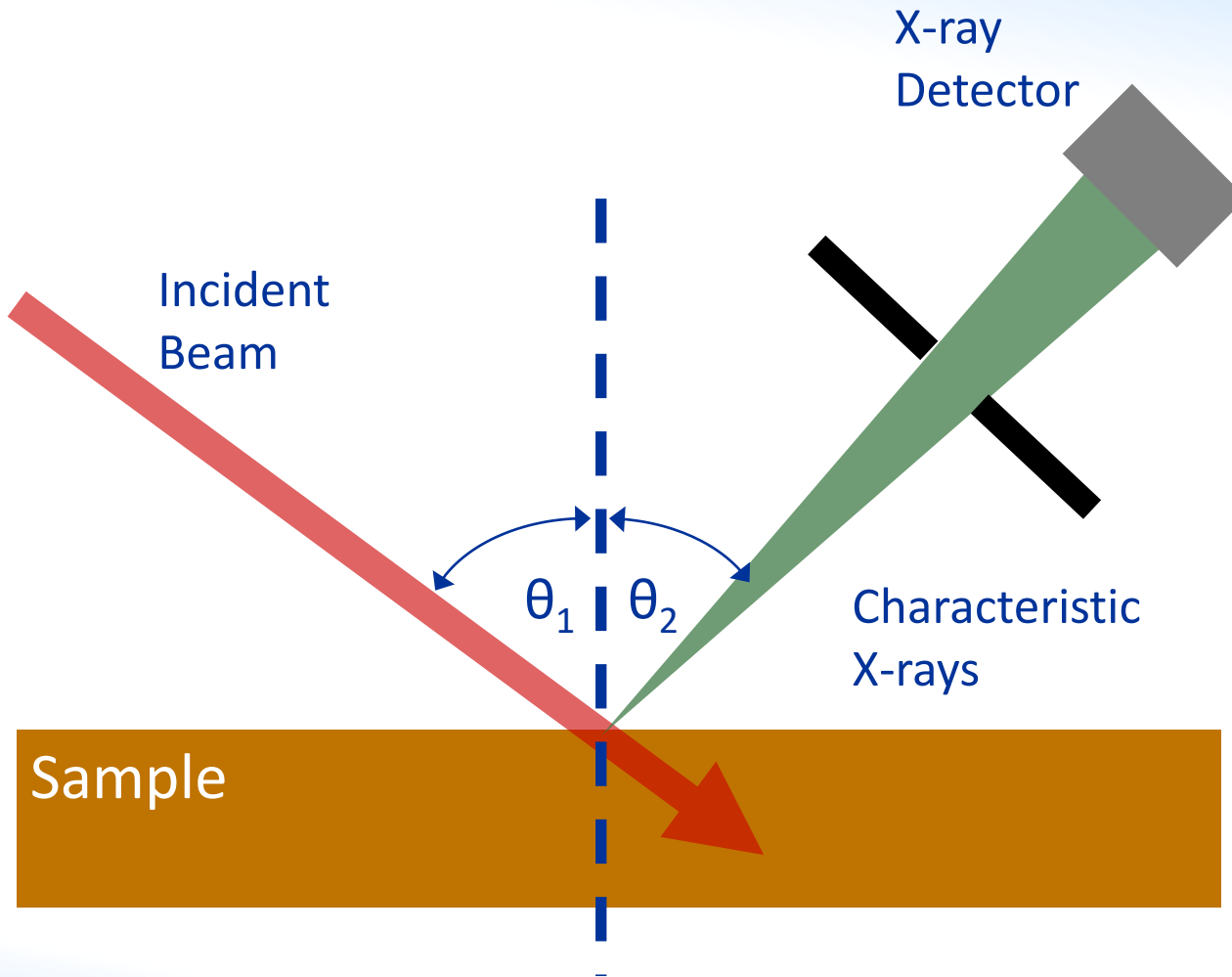
XRF techniques for materials and life sciences

Alessandro Migliori

Nuclear Science and Instrumentation Laboratory

International Atomic Energy Agency

□ Conventional XRF



☐ Sources of ionizing radiation

- Electrons (SEM)
- Charged particles (accelerators)
- Radioisotopes (α , γ , X-rays)
- X-ray Tubes
- Synchrotron radiation

□ Interaction of X-rays with matter

X-rays can interact with the atoms of the material in two different ways:

- **Photoelectric effect**: Primary X-ray radiation can ionise atoms of the material. The X-ray is absorbed in this process
- **Scattering**:
 - ✓ **Elastic/Coherent scattering (Rayleigh)**: no energy loss after collision with electrons. The Rayleigh effect is present when electrons are strongly bound (inner atomic electrons)
 - ✓ **Inelastic/Incoherent scattering (Compton)**: energy loss after collision with electrons. The Compton effect is present when electrons are loosely bound (outer, less bound electrons)

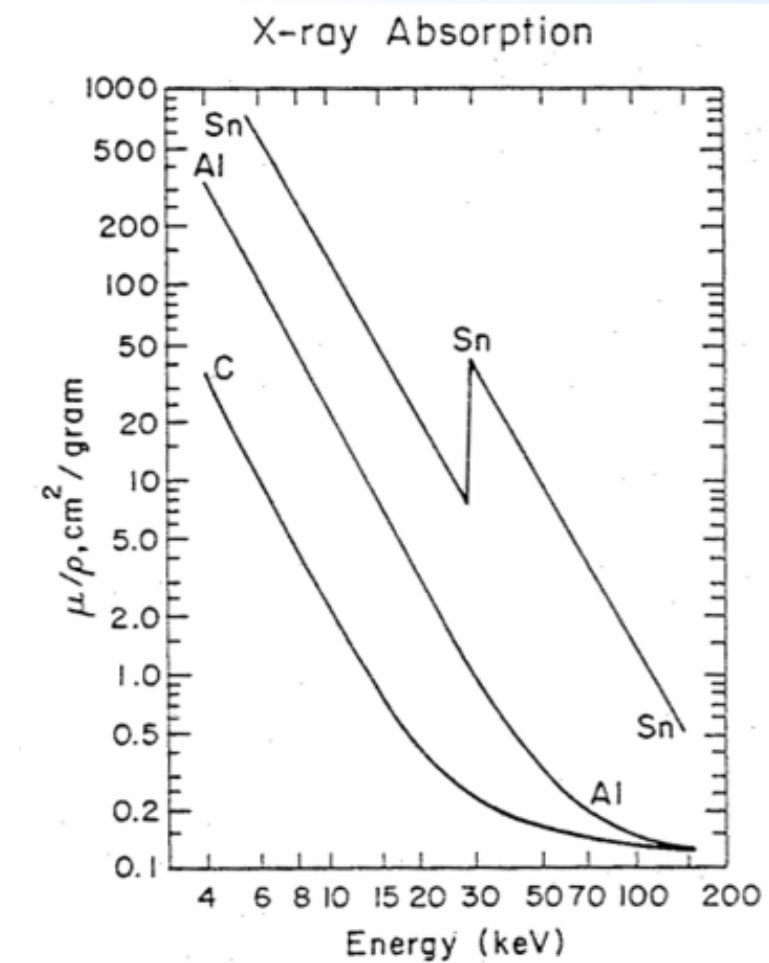
☐ Photoelectric effect

Photoelectric effect: Primary X-ray radiation can ionise atoms of the material to be analysed

Cross section of the PE depends strongly on Z of the material and on the energy of the primary X-ray

$$\sigma_{Ph} \propto \frac{Z^n}{E_X^{3.5}} \quad n = 3 \div 4$$

To maximize the ionization probability, the energy of the primary X-ray should be higher than the binding energy but as close as possible to it



X-Ray Fluorescence

Incident photon
Energy E_0
should be adequate
to ionize the atomic
bound electrons
→ $E_0 \geq$ inner shell
binding energy

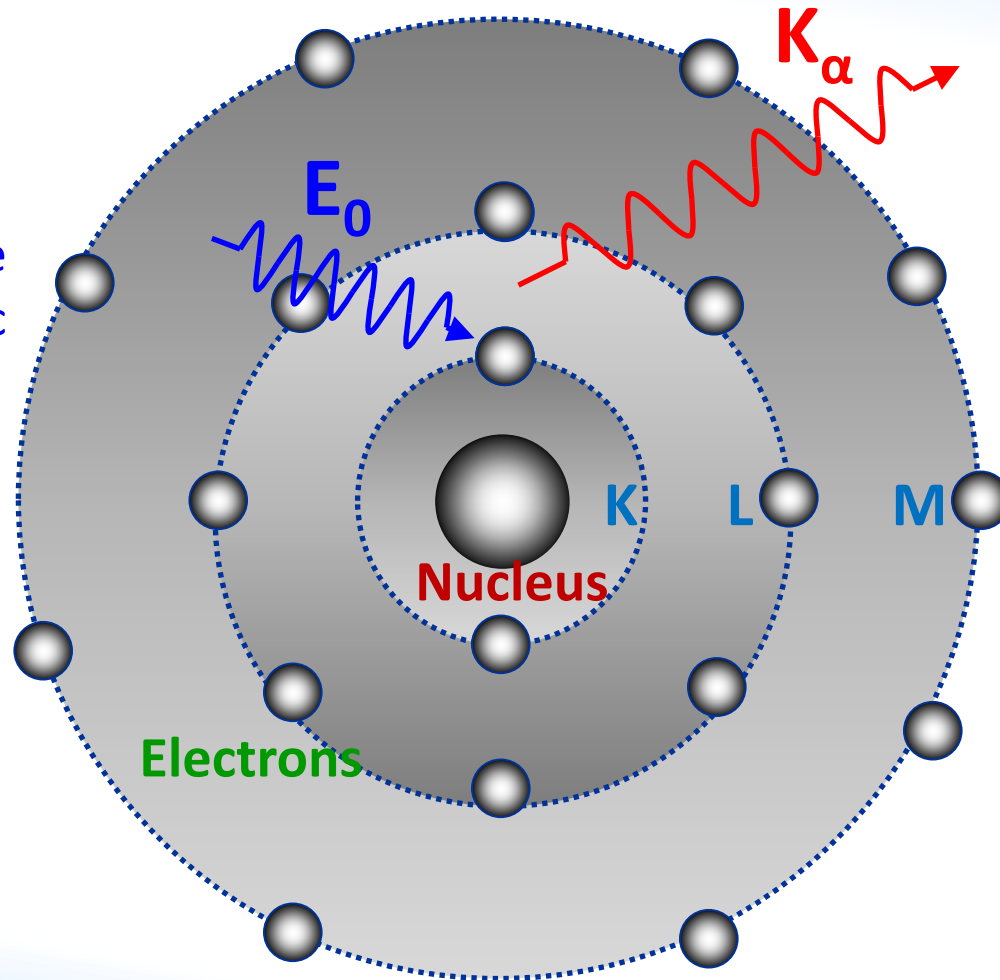
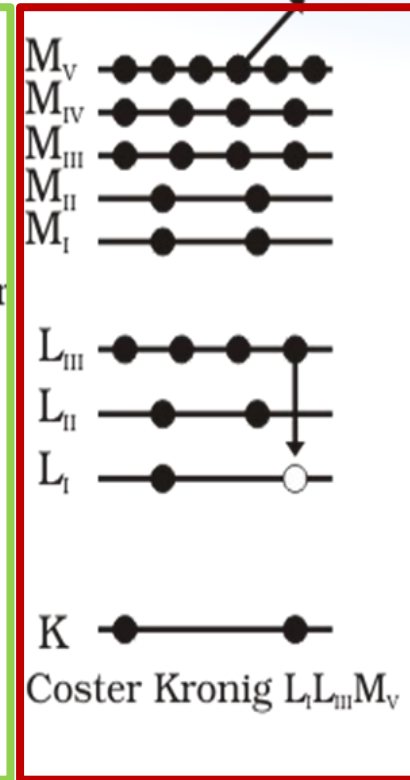
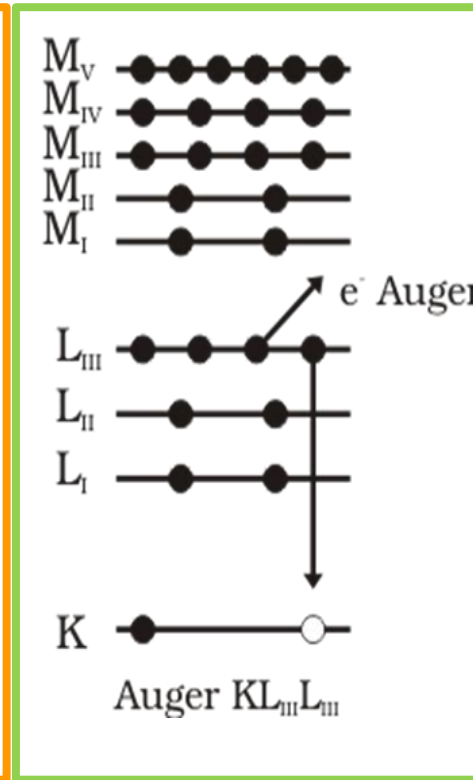
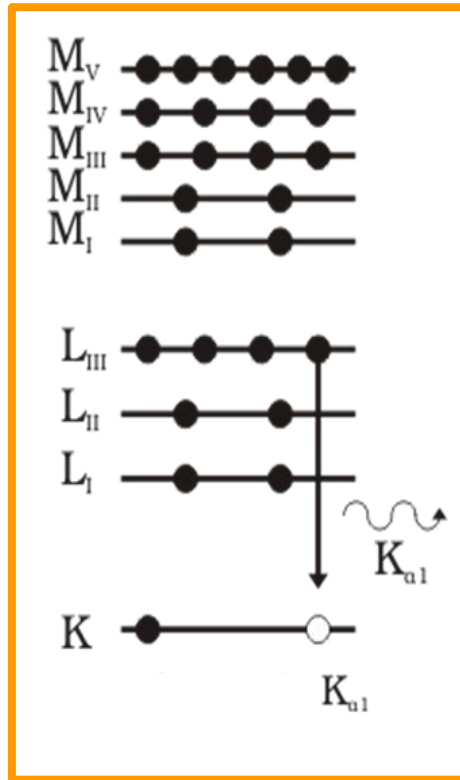


Photo-ionization
of atomic bound
electrons
(K, L, M)
(Photoelectric
absorption)

Electronic
transition and
emission of
element
→ **characteristic
fluorescence
radiation**

Fluorescence
X-ray emission
is **isotropic**

□ De-excitation: Fluorescence/Auger



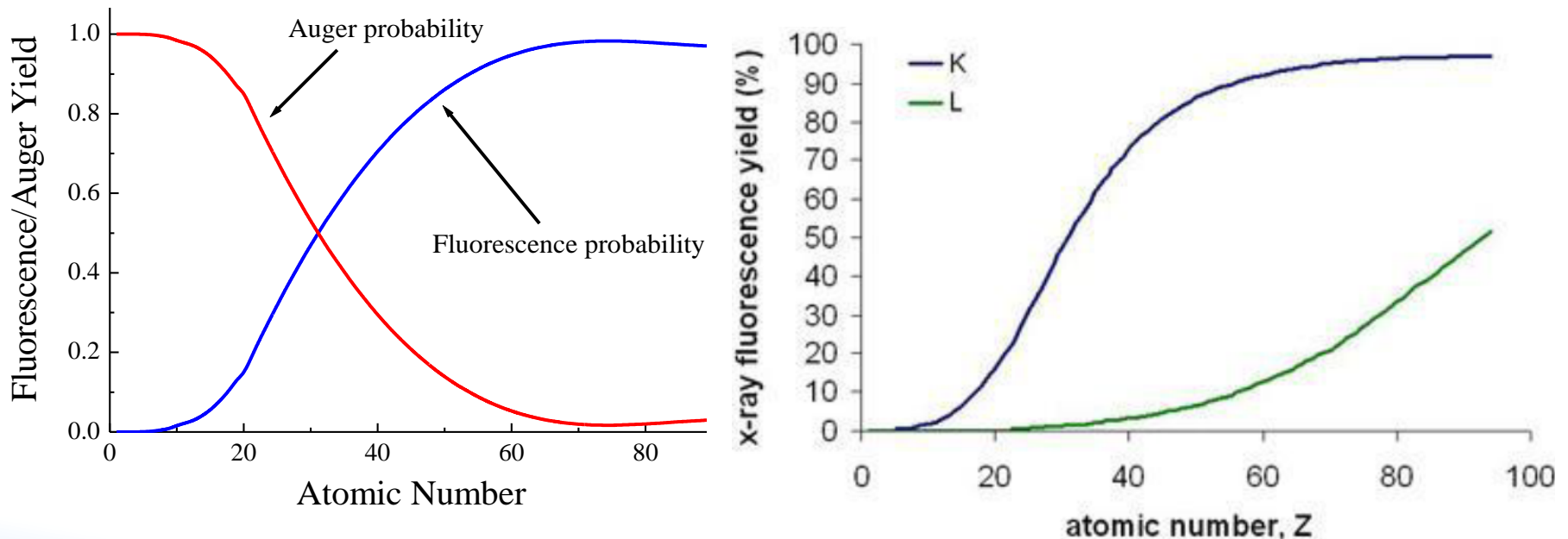
Emission of characteristic X-ray

Emission of electron (vacancy filled by electron from different shell)

Emission of electron (vacancy filled by electron from the same shell)

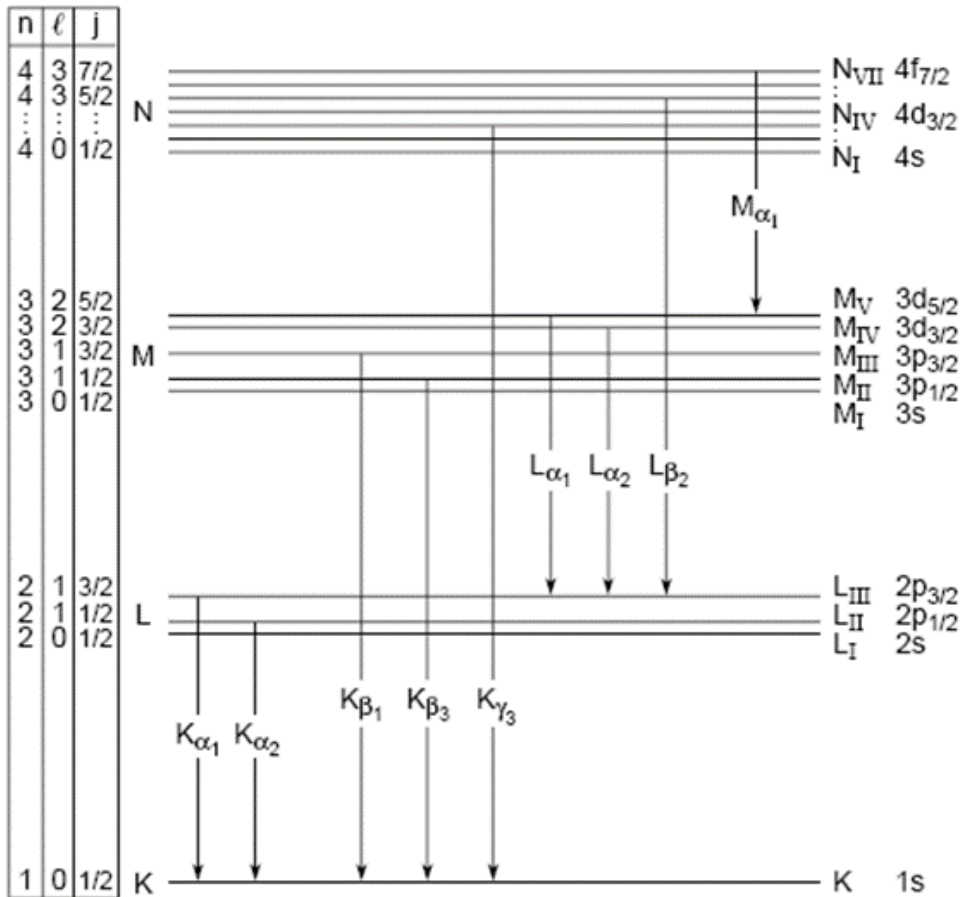
Fluorescence yield

The fluorescence yield is given by the **ratio of the emitted fluorescence photons over the number of the created holes**. The competing process is the **emission of Auger electrons** as the atom returns to its ground state



For low Z the Auger electron emission is dominant

□ Emission of characteristic X-rays



The emission of characteristic X-ray lines follows allowed electronic transitions between specific subshells. Each element has a unique set of emission lines.

Siegbahn/IUPAC notation:

K_{α} : K-L₂ + K-L₃

K_{β} : K-M₂ + K-M₃

L_{α} : L₃-M₄ + L₃-M₅

L_{β_1} : L₂-M₄

L_{β_2} : L₃-N₅

□ X-ray energies

Moseley's law

$$E = h \cdot A \cdot R \cdot (Z - b)^2$$

h = Planck constant

R = Rydberg frequency

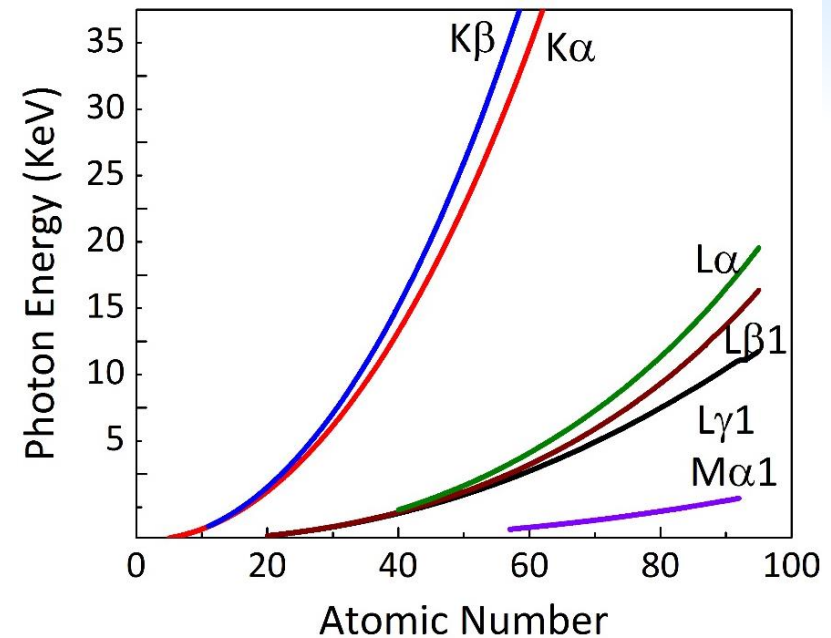
Z = atomic number

$A = 3/4$ for K_α , $5/36$ for L_α

$b = 1$ for K_α , 7.4 for L_α

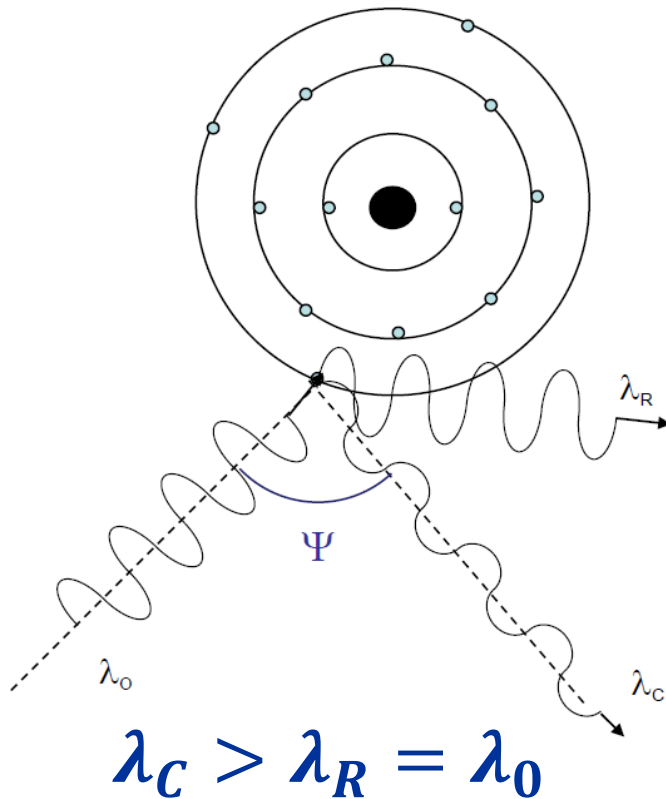
K_α	$E \text{ [eV]} \approx 10.20 \cdot (Z - 1)^2$	$E_{Fe-K\alpha} \approx 6380 \text{ eV}$
------------	--	--

L_α	$E \text{ [eV]} \approx 1.89 \cdot (Z - 7.4)^2$	$E_{Pb-L\alpha} \approx 10520 \text{ eV}$
------------	---	---



X-ray spectroscopy within the energy range 1÷30 keV offers in principle the possibility to detect all the periodic table elements ($Z > 10$) through their K, L or even M series of emission lines

□ X-ray scattering



Elastic/coherent scattering (Rayleigh):

no energy loss after collision with electrons. The Rayleigh effect is present when electrons are strongly bound.

Rayleigh is more intense for high Z (= heavy) matrices

Inelastic/incoherent scattering (Compton):

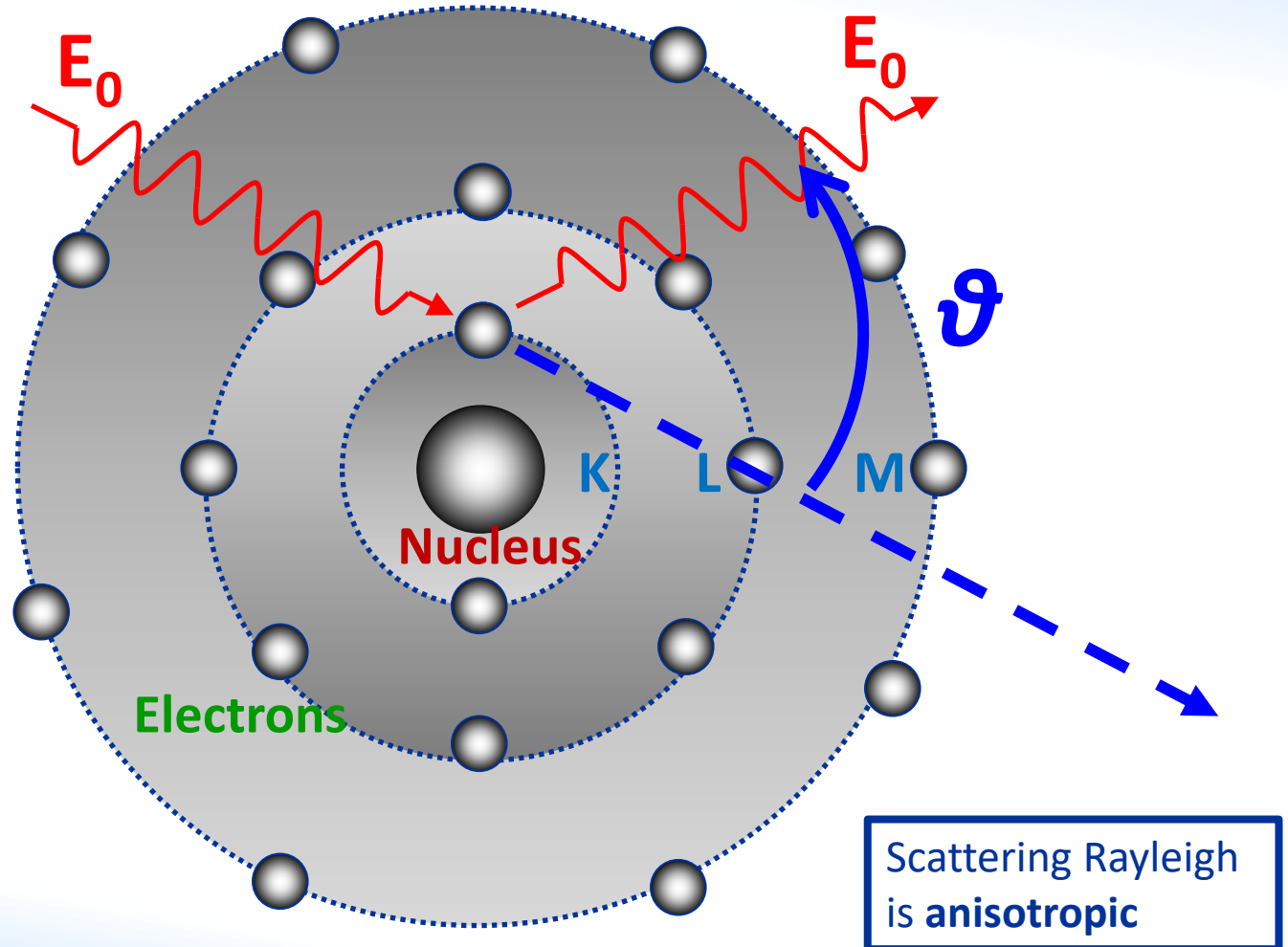
energy loss after collision with electrons. The Compton effect is present when electrons are loosely bound.

Compton is more intense for low Z (= light) matrices

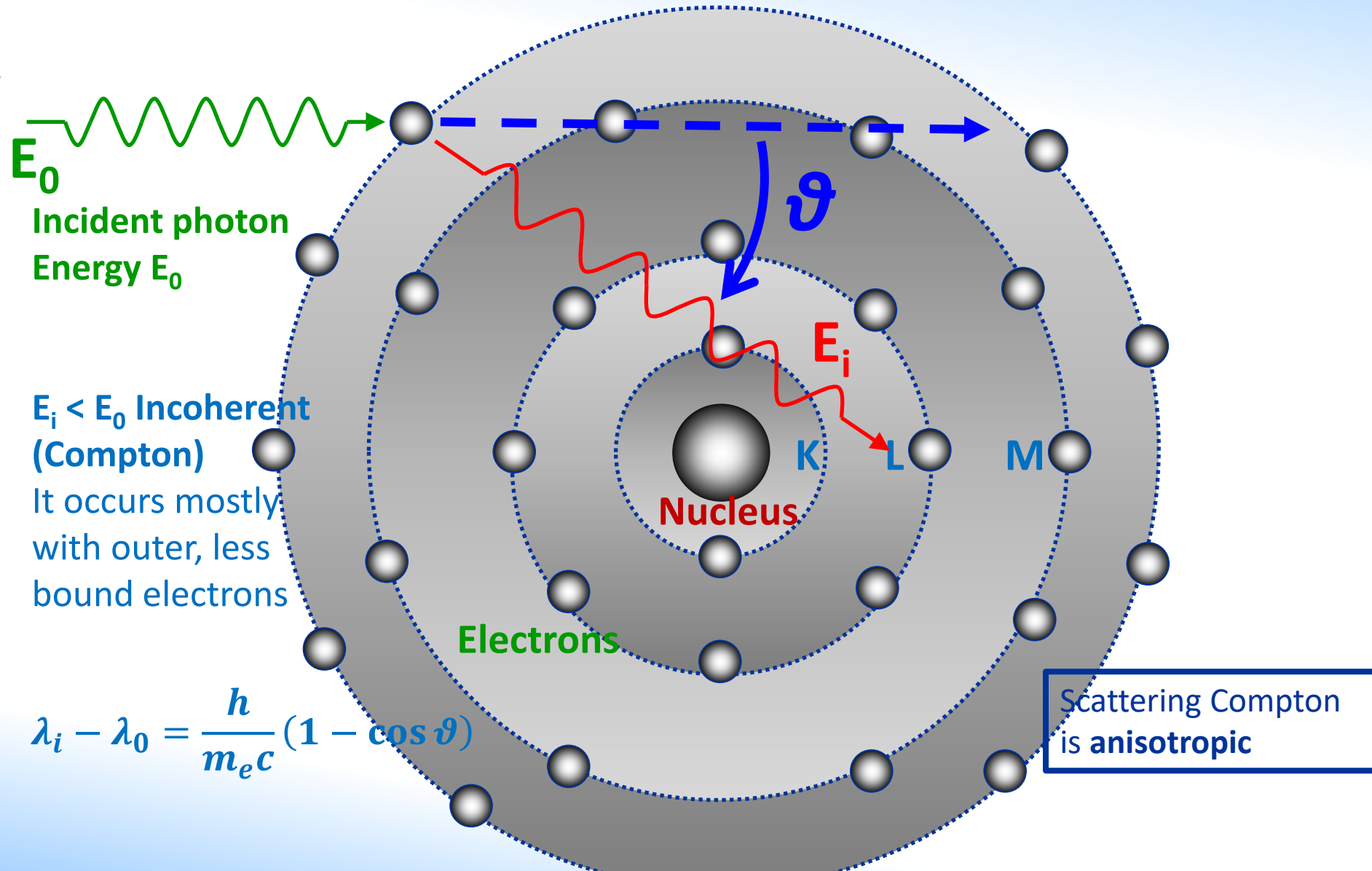
□ Rayleigh scattering

Incident photon
Energy E_0

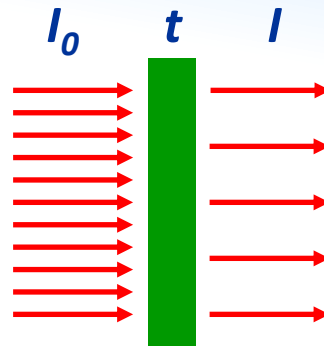
$E_i = E_0$: Coherent
(Rayleigh)
It occurs mostly
with inner atomic
electrons



Compton scattering



□ Linear attenuation coefficient μ



Attenuation of photons by a thin layer of thickness dt is described by

$$dI = I \cdot \mu \cdot dt$$

where I is the number of photons per unit area and unit time (photon flux) of which dI are attenuated while penetrating the layer of a material characterized by the **(total, linear) attenuation coefficient μ** . This is equivalent to

$$I = I_0 \cdot e^{-\mu \cdot t}$$

I and I_0 are the photon fluxes behind and in front of the absorber, respectively, and t is the thickness. μ is a function not only of the material (atomic number Z) but also of the photon energy E

□ Mass attenuation coefficient μ_m

$$\mu = \mu_m \cdot \rho$$

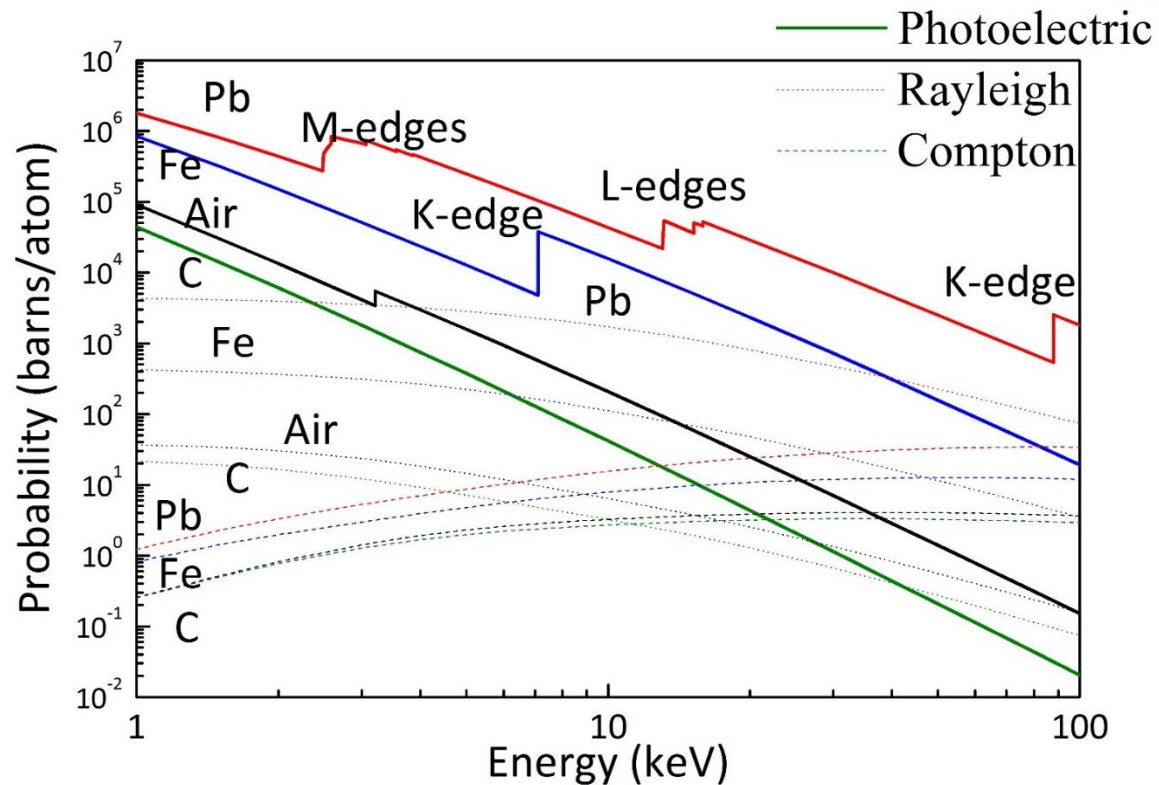
the total mass attenuation coefficient μ_m doesn't depend on the density ρ of the material.

The coefficient μ_m summarizes all possible photon interactions

$$\mu_m = \tau_m + \sigma_m$$

where τ_m describes the photo absorption and $\sigma_m = \sigma_{coh} + \sigma_{inc}$ are the contributions by coherent and incoherent scattering, respectively.

Both kinds of scattering contribute much less than the photo absorption to the total μ_m



□ Mass attenuation coefficient μ_m

the mass attenuation coefficient of a material that is composed of several elements, with weight fractions w_i , is

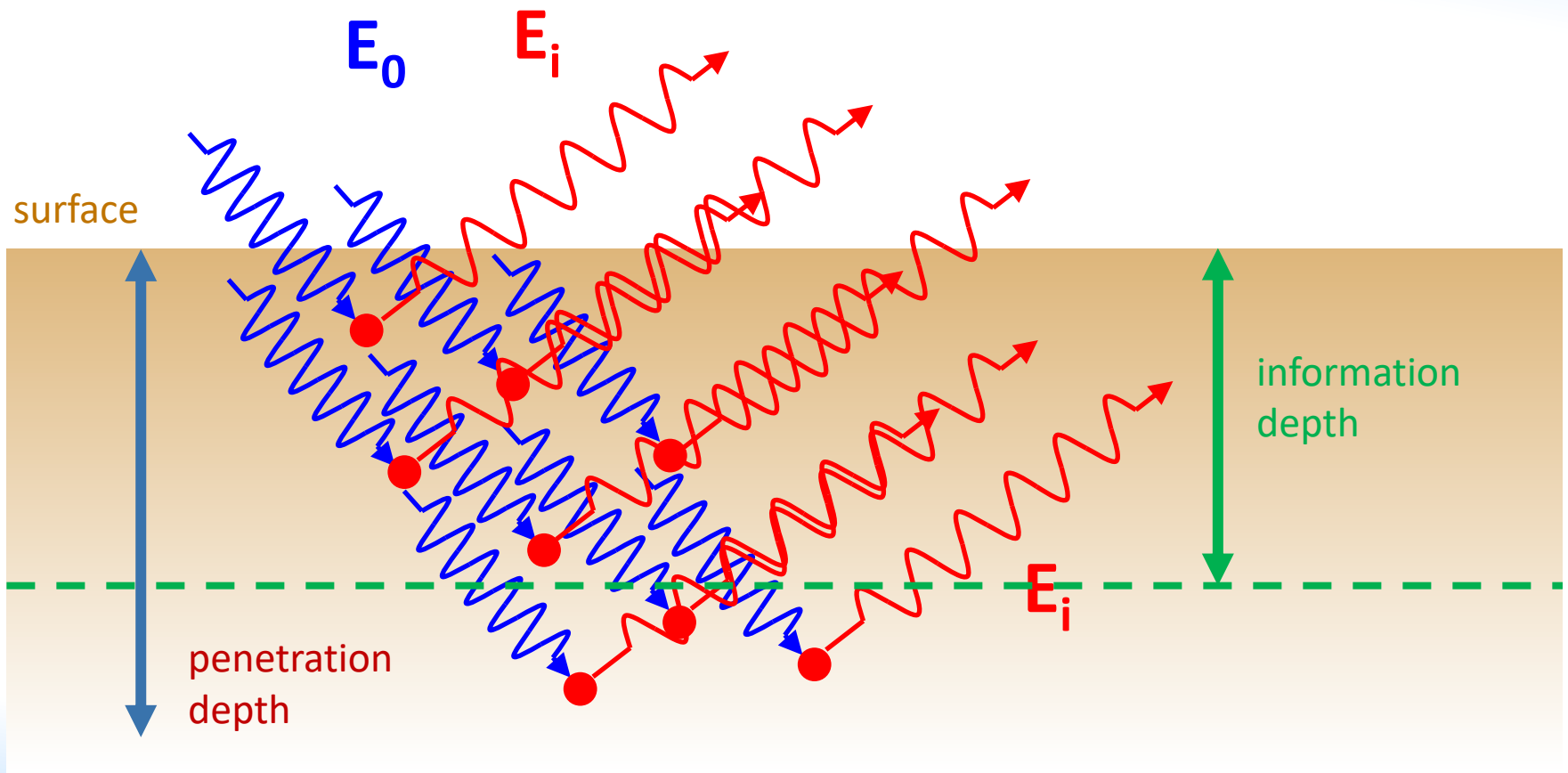
$$\mu_m = \sum_i w_i \cdot \mu_m^i$$

Use of mass attenuation coefficients suggests replacing the thickness by the **area-related mass** $m = M/A$ (mass M per unit area A) and rewriting the attenuation law as

$$I = I_0 \cdot e^{-\mu_m \cdot m}$$

$t \cdot \rho = M/A$, in **grams/cm²**

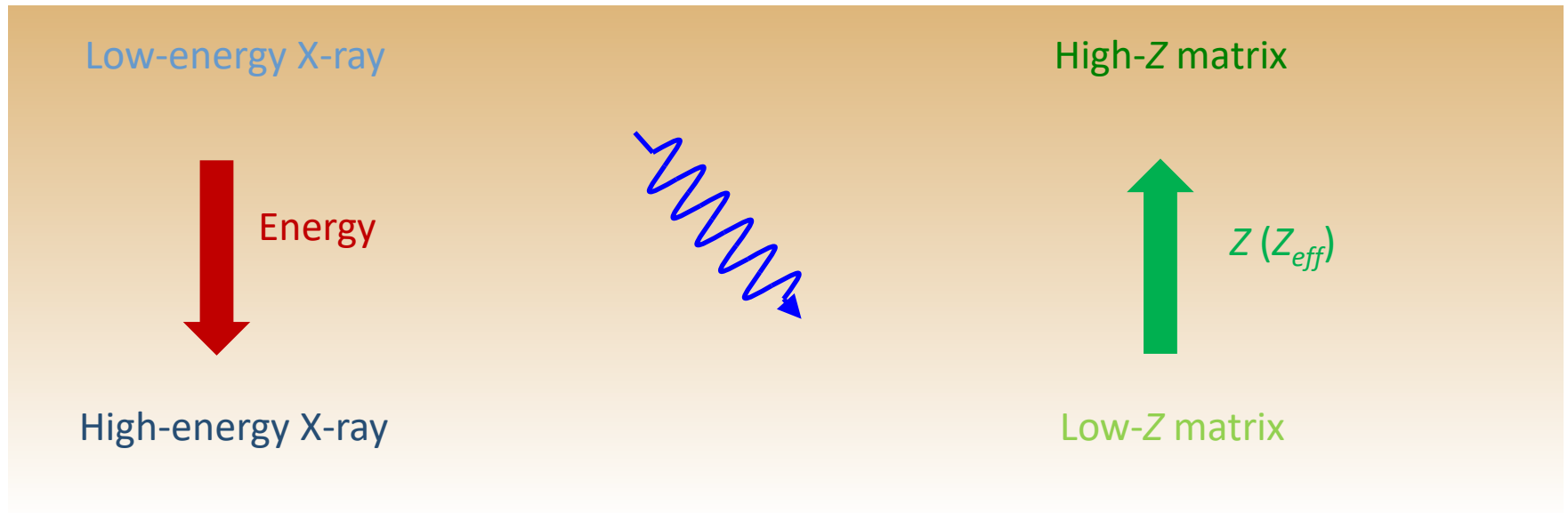
□ Penetration and information depth



□ Penetration and information depth

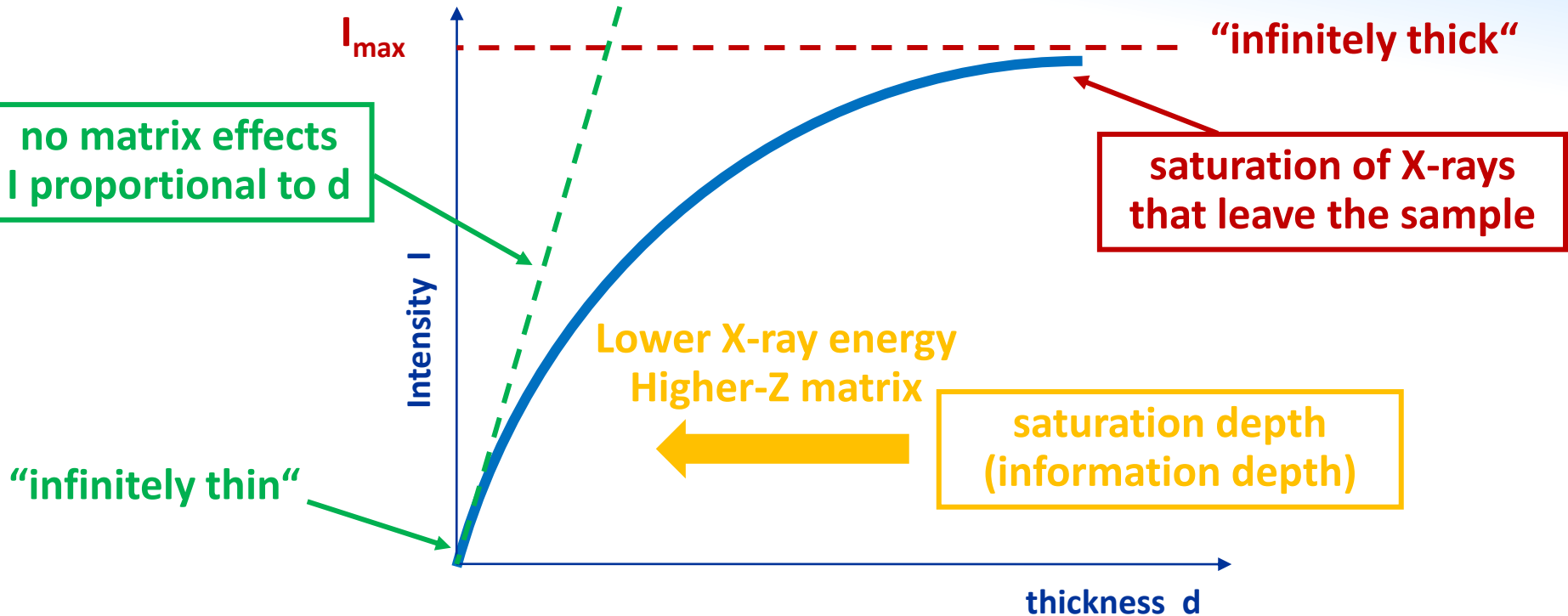
Penetration and information (analytical) depth depend on the energy of the X-ray and on the matrix:

surface



- **Surface treatment is extremely important for heavy matrices**
- **Information thickness is essential for light matrices**

□ Influence of sample thickness



Increasing the thickness of the sample above the information depth will not increase the signal but only the scattering of the primary radiation

□ Analytical depths in different matrices

Different elements exhibit different Information thicknesses (99%), depending on their characteristic X-ray energy and on the overall matrix

Line	Energy	Graphite	Glass	Iron	Lead
Cd K _{α1}	23,17 keV	14,46 cm	8,20 mm	0,70 mm	77,30 μm
Mo K _{α1}	17,48	6,06	3,60	0,31	36,70
Cu K _{α1}	8,05	5,51 mm	0,38	36,40 μm	20,00
Ni K _{α1}	7,48	4,39	0,31	29,80	16,60
Fe K _{α1}	6,40	2,72	0,20	*164,00	11,10
Cr K _{α1}	5,41	1,62	0,12	104,00	7,23
S K _{α1}	2,31	116,00 μm	14,80 μm	10,10	4,83
Mg K _{α1}	1,25	20,00	7,08	1,92	1,13
F K _{α1}	0,68	3,70	1,71	0,36	0,26
N K _{α1}	0,39	0,83	1,11	0,08	0,07
C K _{α1}	0,28	*13,60	0,42	0,03	0,03
B K _{α1}	0,18	4,19	0,13	0,01	0,01

$$E_{Kc} = 0.2842$$

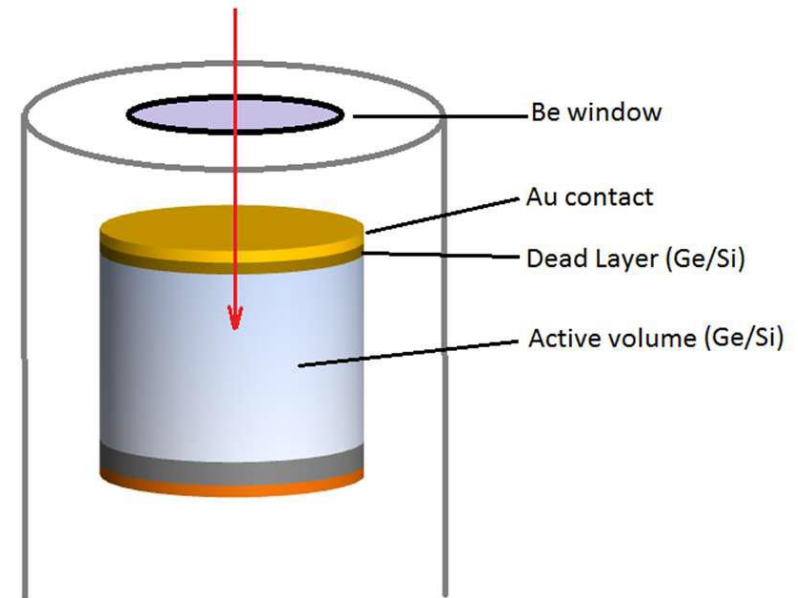
$$E_{KFe} = 7.112$$

Detectors

- Proportional Counters
- Scintillation Detectors
- Si(Li)
- LEGe
- PIN Diode
- **SDD**
- CCD, CMOS cameras
- CZT, other

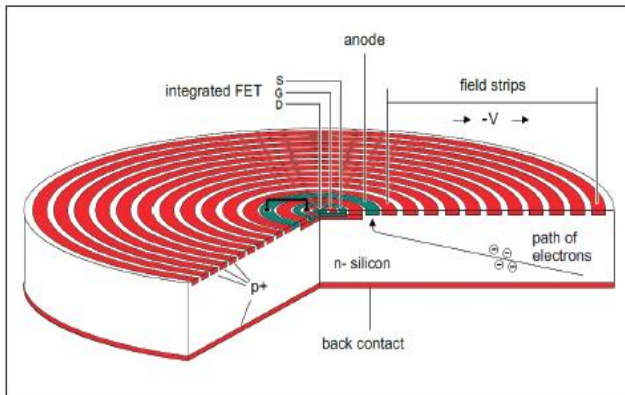
□ Semiconductor detectors

- X-rays produce **electron-hole pairs**, whose number is **proportional** to the energy of the radiation (average energy to produce an electron/hole pair is 3.6eV for Si and 2.9eV for Ge)
- Electrons and holes are collected from the depleted active region to the electrodes, where they result in a **pulse** that can be further **amplified** and finally **measured**
- This pulse carries information about the energy of the original incident radiation. The number of such pulses per unit time also gives information about the intensity of the radiation



□ Silicon Drift Detectors - SDD

The charge is drifted from a large area into a small read-out node with low capacitance, independent of the active area of the sensor. Thus, the serial noise decreases, and shorter shaping time can be used. For SDDs faster counting is enabled and higher leakage current can be accepted, drastically reducing the need for cooling.

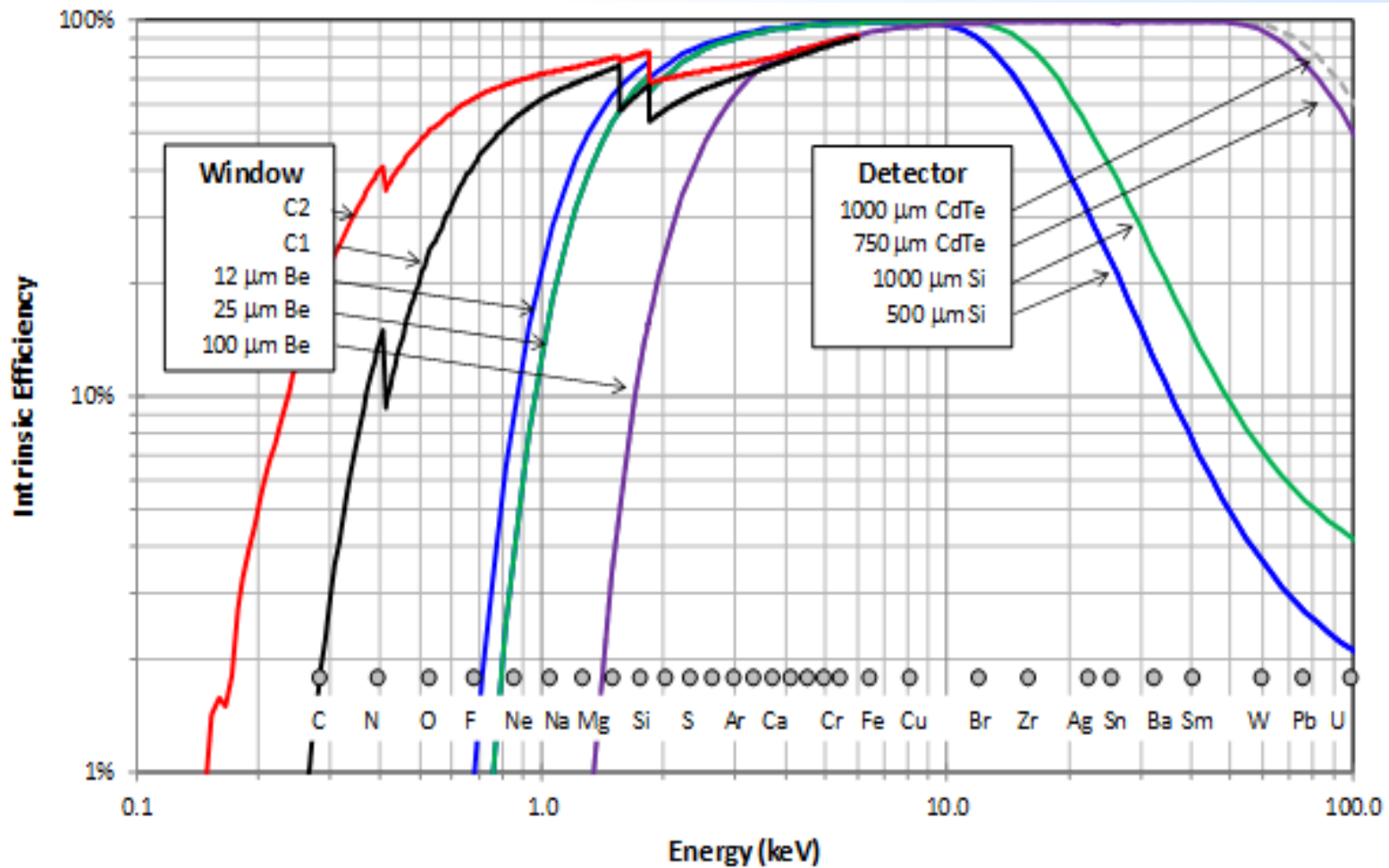


- Energy resolution $\sim 125 - 140$ eV (Mn-Ka)
- Input capability $\sim 10^6$ photons/sec

https://tools.thermofisher.com/content/sfs/brochures/TN52342_E_0512M_SiliconDrift_H.pdf

Detector photograph reproduced from <https://www.rayspec.co.uk/x-ray-detectors/silicon-drift-detectors/xrf/>

Efficiencies of different detectors

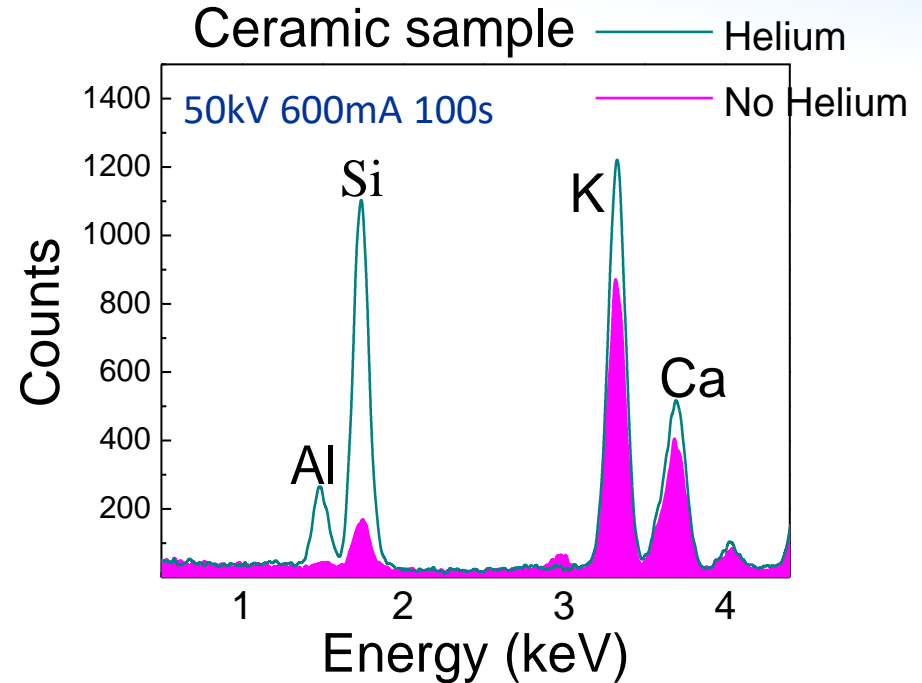
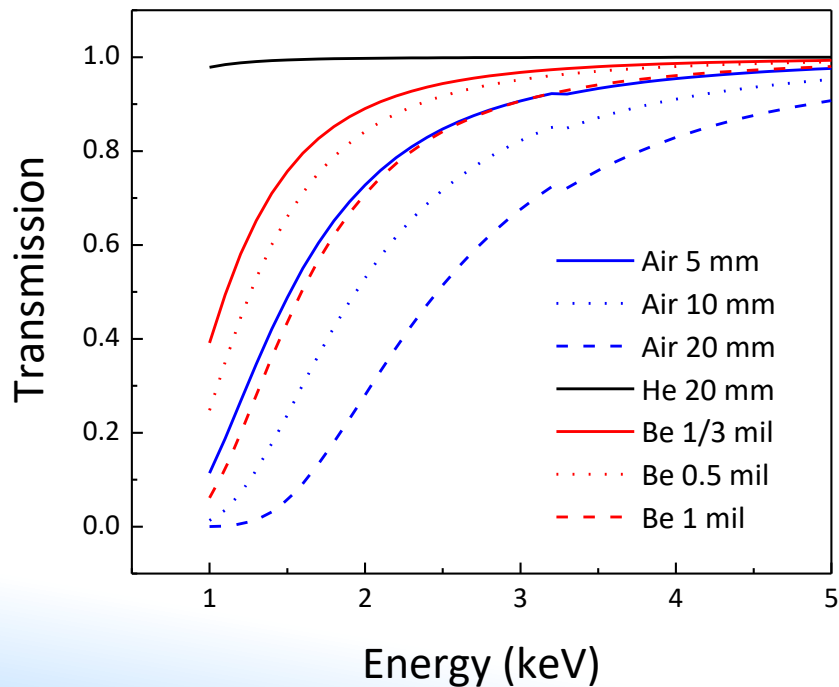


Comparison of different detector's efficiency from AMPTEK

<https://www.amptek.com/products/x-ray-detectors/fastssdd-x-ray-detectors-for-xrf-eds/fastssdd-silicon-drift-detector>

☐ “Light” elements (Na, Mg, Al, Si)

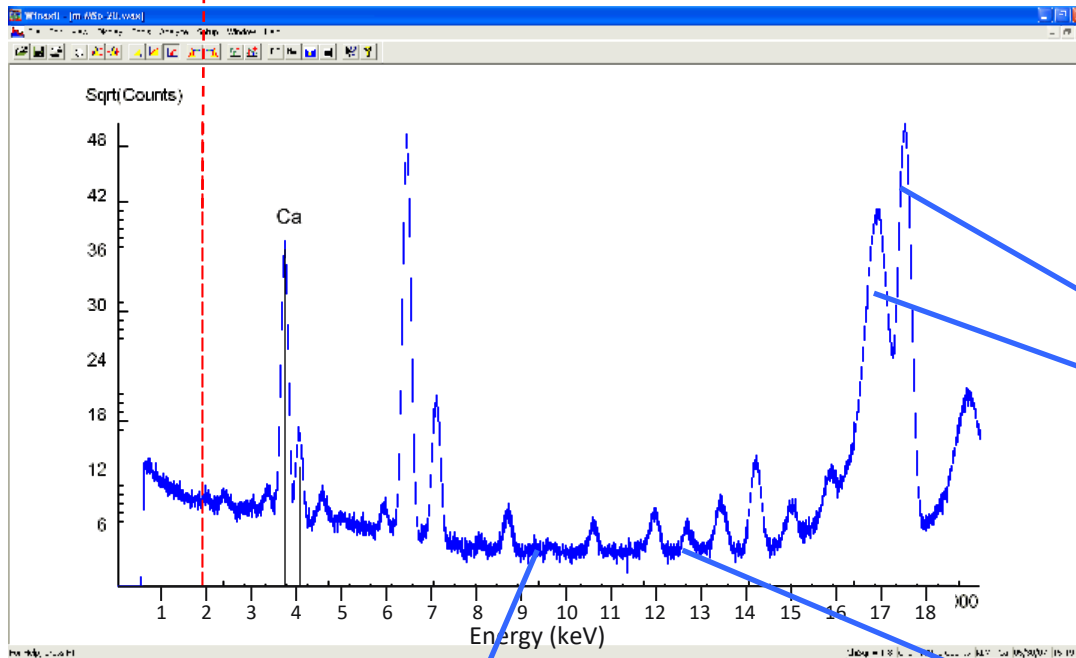
Vacuum atmosphere or He flushing is required in the x-rays path between sample and detector



The improvement in the intensity of Al-K and Si-K characteristic X-ray lines is significant, 22 and 7.3 times respectively

□ Typical EDXRF spectrum

- Escape peaks (Ca-Ka – 1.74 keV = 1.95 keV)



- Characteristic radiation
✓K, L or M-lines

- Scatter
✓Coherent
✓Incoherent

- Sum peaks
Fe-Ka + Fe-Ka= 12.8 keV

- Continuum radiation

Resolution of EDXRF spectrometers

Full Width at Half Maximum (FWHM) of a peak

$$FWHM_{Peak}^2 = FWHM_{Elec}^2 + FWHM_{Det}^2$$

Electronic noise:
~100 eV

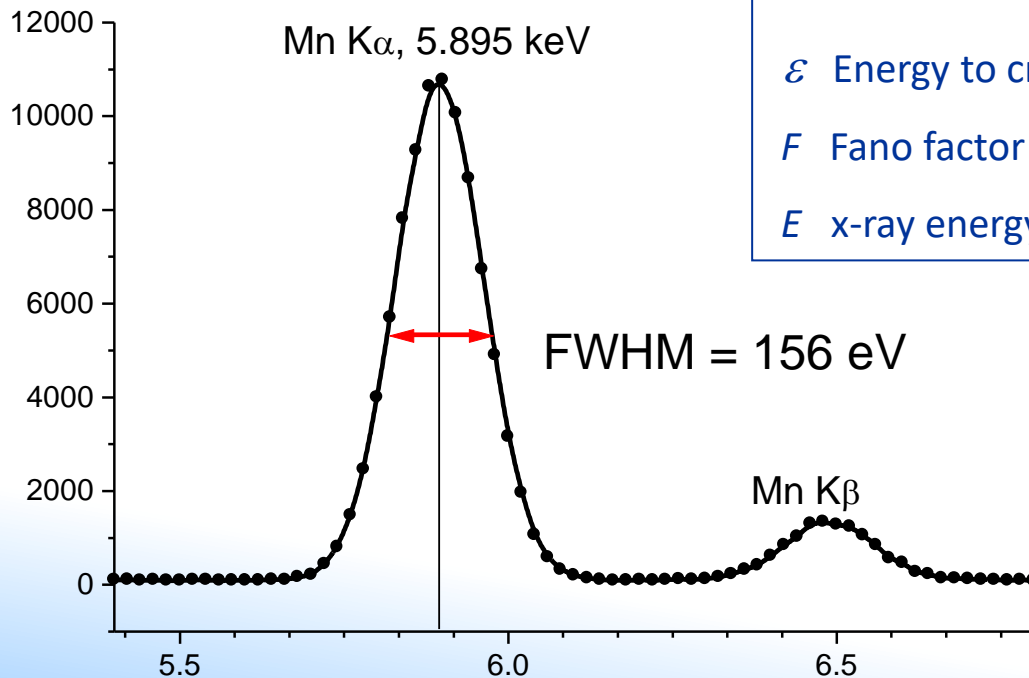
Intrinsic contribution:

$$2.3548 \sqrt{\epsilon \times F \times E}$$

ϵ Energy to create e-h pair (3.85 eV)

F Fano factor (~0.114)

E x-ray energy in eV



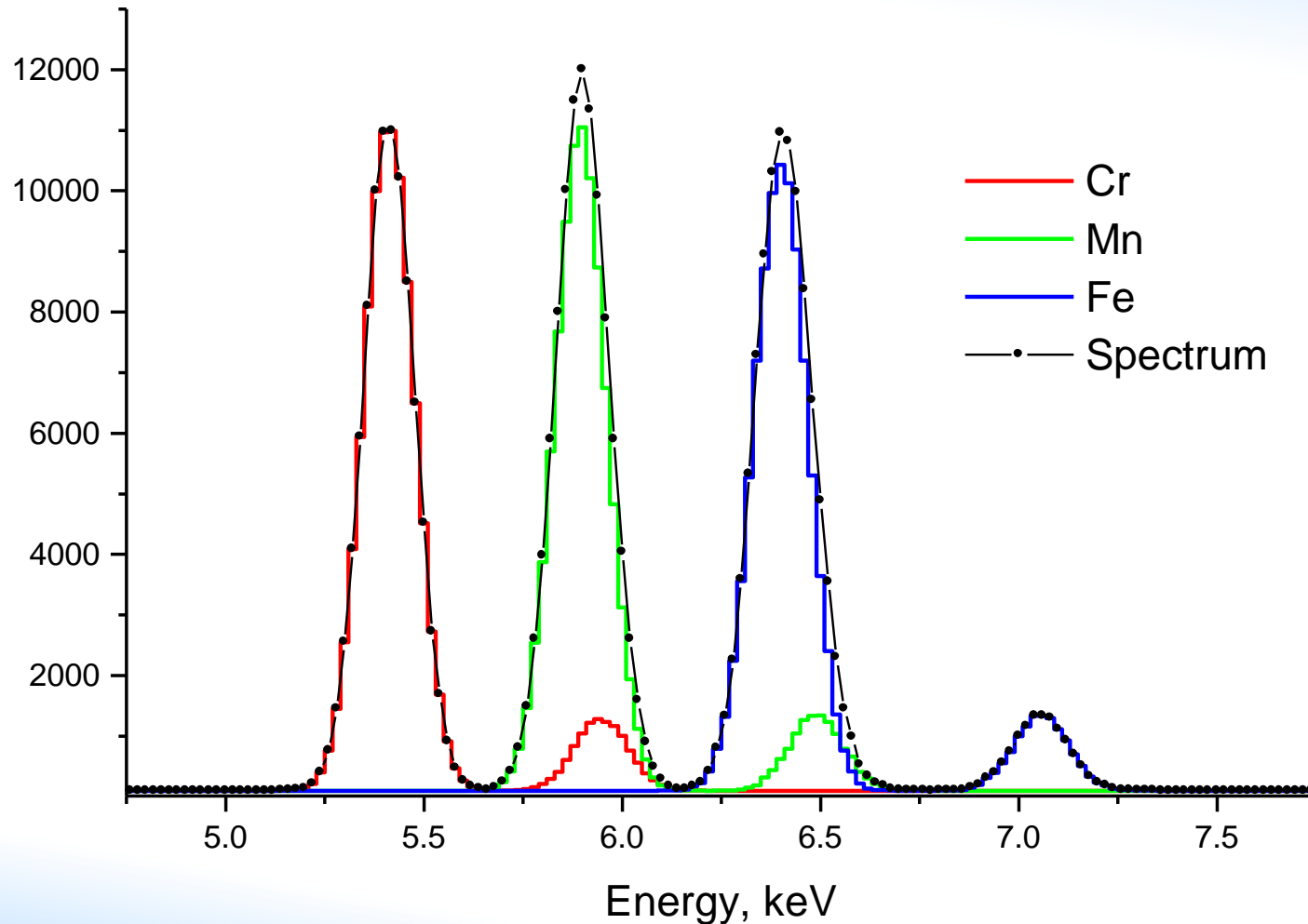
Mn K α @ 5.895 keV

$FWHM_{Det} = 120$ eV

$FWHM_{Elec} = 100$ eV

$\Rightarrow FWHM_{Peak} = 156$ eV

□ Cr-Mn-Fe overlap at ~160 eV



□ Case of strong overlapping

Overlapping of As-K α (about 10.54 keV) and Pb-L α lines (about 10.55 keV)

Binding energies:

As-K = 11.87keV

Pb-L₃ = 13.04keV

Pb-L₂ = 15.20keV

Pb-L₁ = 15.86keV

Arsenic can be easily quantified at synchrotron using an energy
 $11.87 \text{ keV} < E < 13.04 \text{ keV}$

□ The Shermann-Nikina formulae

$$I_i = \varepsilon(E_i) w_i \int_{E > E_i^{ab}}^{E_{\max}} G K_i A(E_0, E_i) R_i(E_0, E_j) I_0(E_0) dE_0$$

$$K_i = \frac{J_K^i - 1}{J_K^i} \omega_K^i f_{K\alpha}^i \tau_i(E_0)$$

Contains all the fundamental parameters for specific k-line of element i

$$A_S(E_0, E_i) = \frac{1 - e^{-\chi_S(E_0, E_i)\rho x}}{\chi_S(E_0, E_i)}$$

Takes into account the attenuation of both excitation and fluorescent radiation in the sample

$$R_i(E_0, E_j)$$

Considers the enhancement of x-ray production of element i by the characteristic of other major elements j present in the sample and having characteristic energies larger than absorption edge of element i

$$I_0(E_0)$$

Is the probability distribution by energies of the excitation radiation

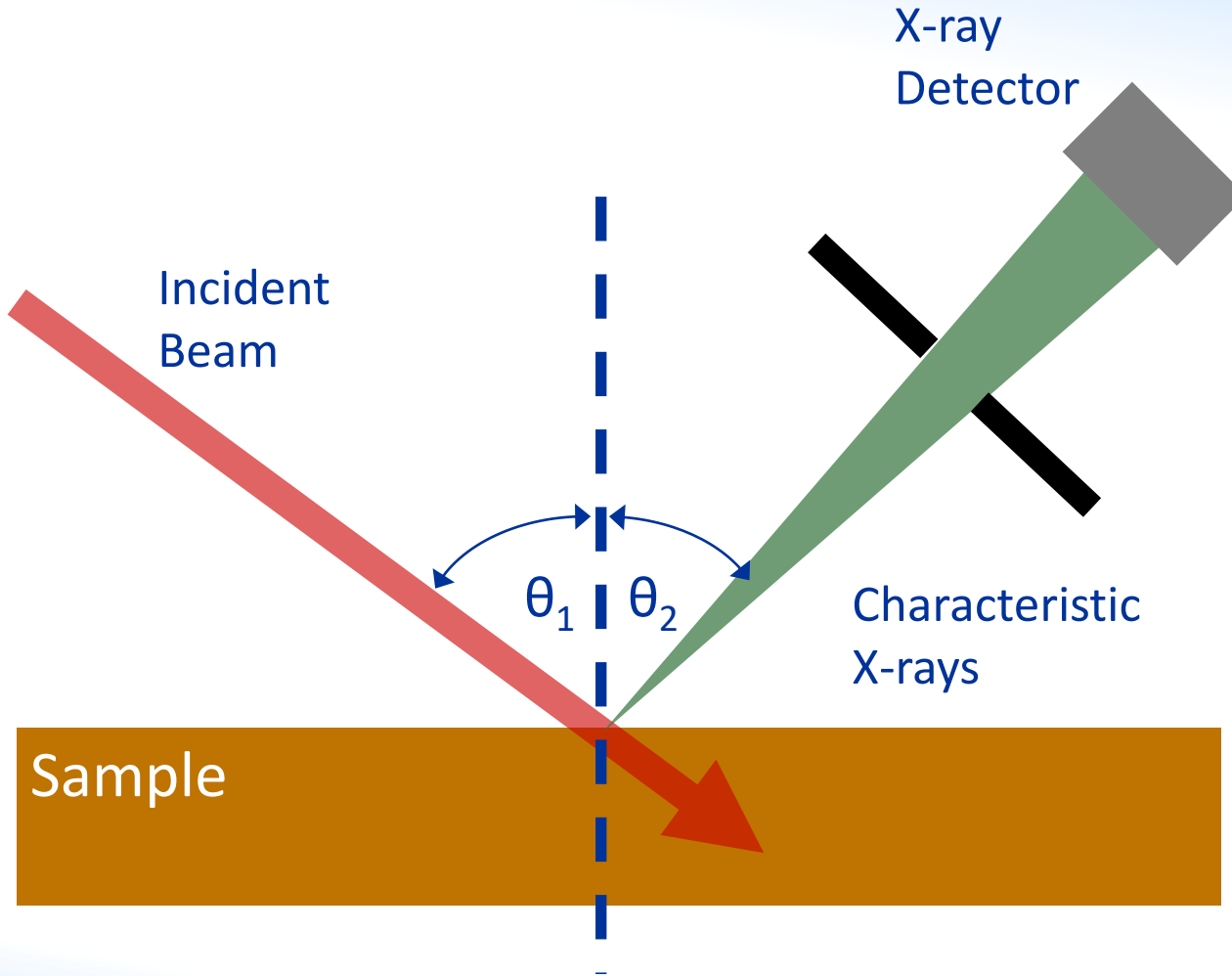
$$\varepsilon(E_i)$$

Is the efficiency of the detector for energy E_i

$$G$$

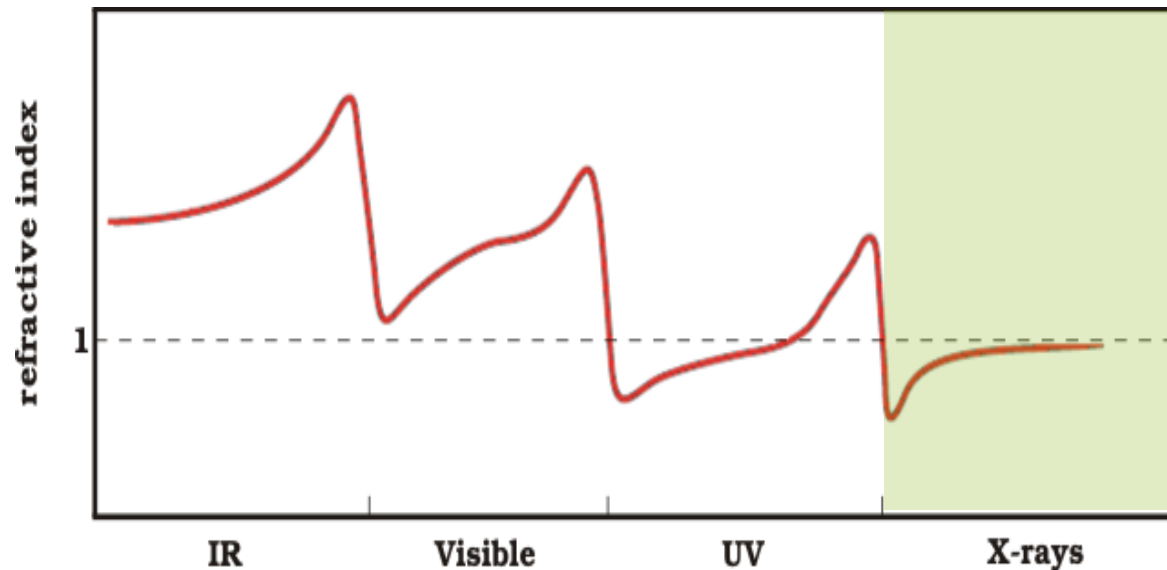
Is the overall effective solid angle for excitation and detection

□ Conventional XRF



X-ray optics

Refractive index: $n = \frac{c}{u_p}$

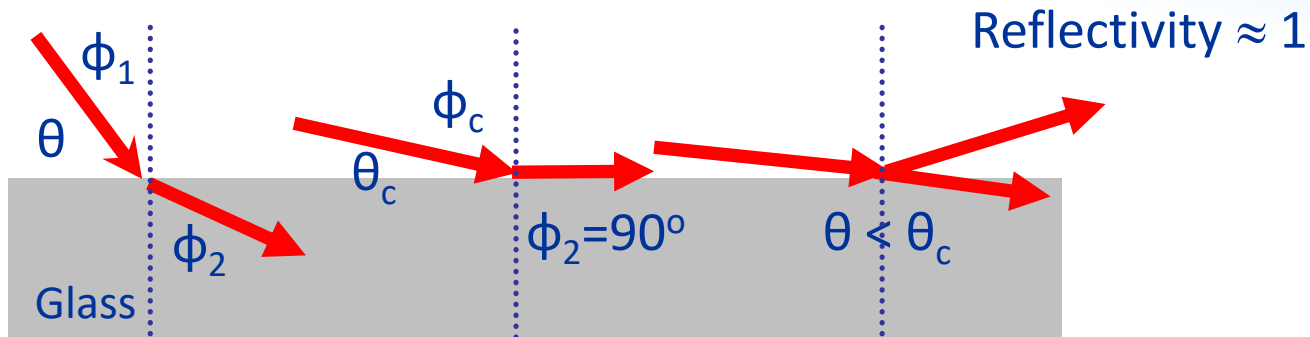


$$n = 1 - \delta + i\beta$$

β = Attenuation term

δ = Phase term

□ X-ray total reflection

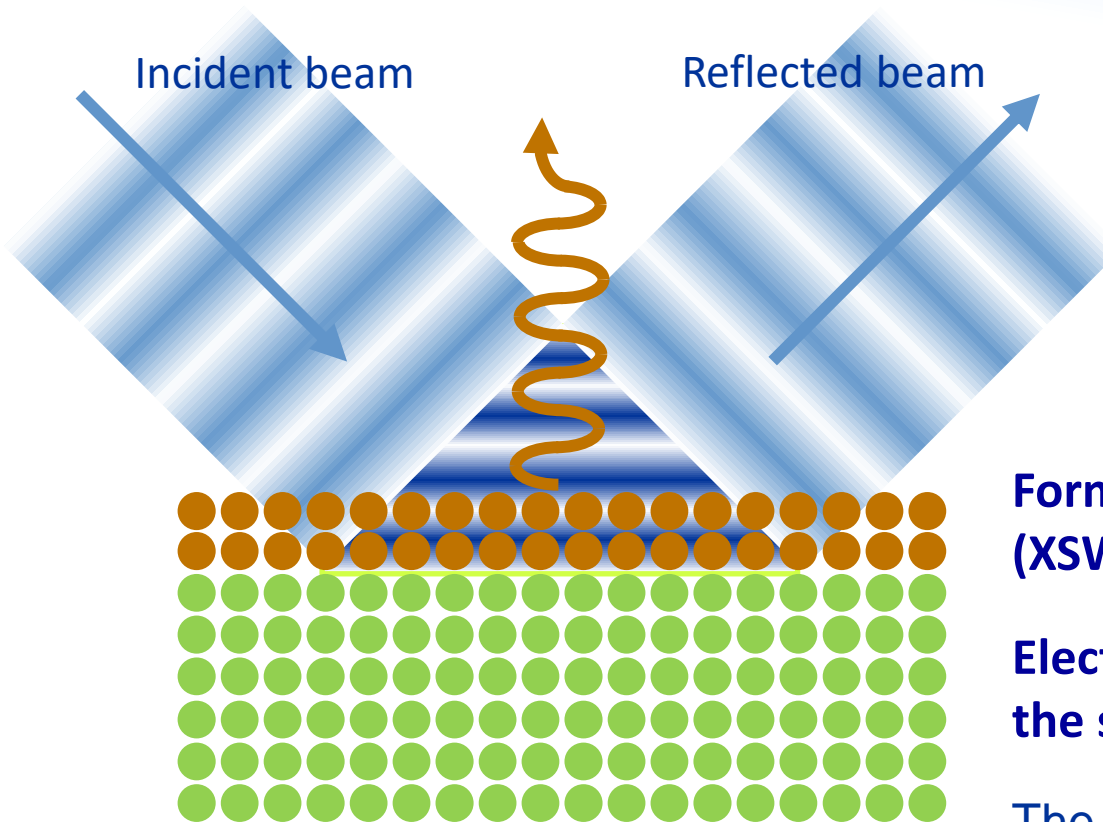


Snell Law $\frac{\sin \phi_2}{\sin \phi_1} = \frac{1}{n} \Rightarrow \sin \phi_2 = \frac{\sin \phi_1}{n} \Rightarrow \phi_2 > \phi_1 \quad n \approx 1 - \delta$

$$\vartheta_{crit} = \sqrt{2\delta} \quad \vartheta_{crit}(deg) \approx \frac{1.651}{E(keV)} \sqrt{\frac{Z}{A} \rho(\frac{g}{cm^3})}$$

Z: Atomic number
 A: Atomic mass
 ρ : Density

□ X-ray Standing Wave



Formation of X-ray Standing Wave (XSW) at grazing incident/exit angle

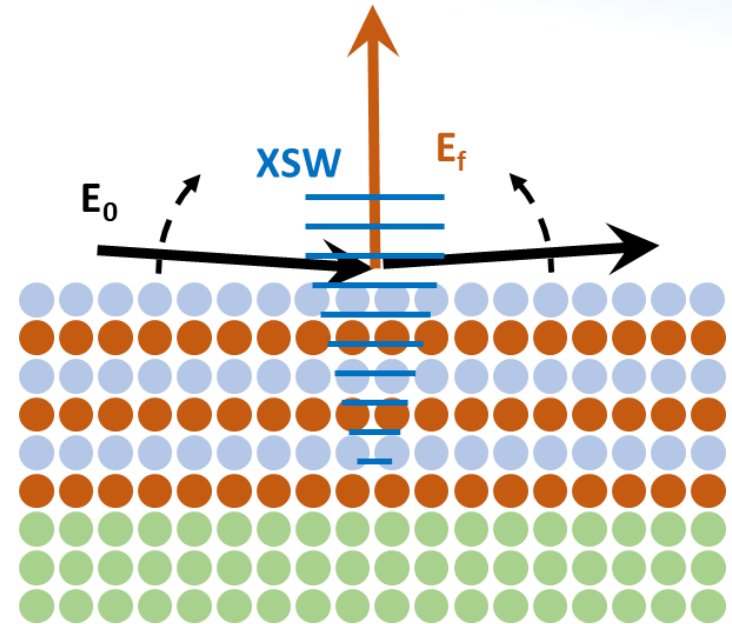
Electric Field Modulations above the surface

The X-ray fluorescence intensity from the sample depends on the varying field intensity of the XSW field within the sample

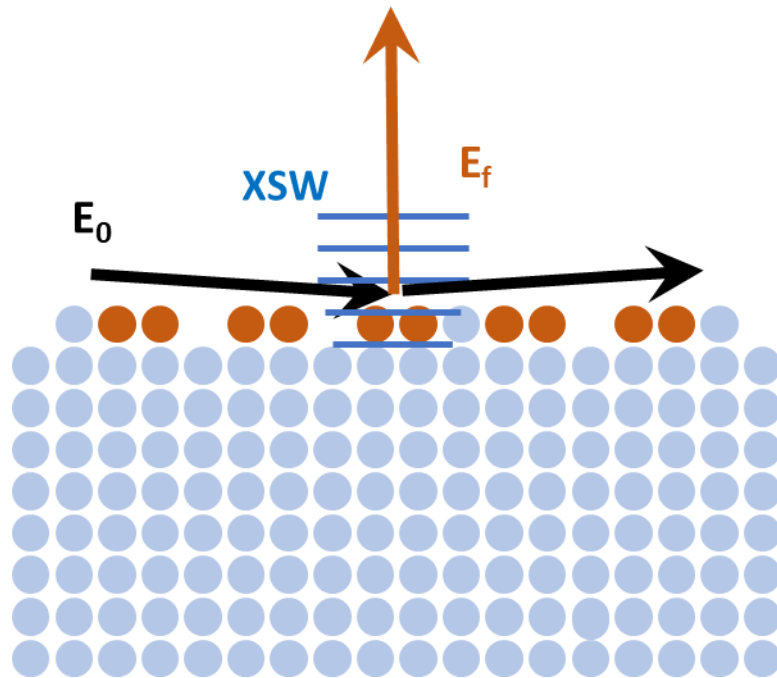
□ GIXRF and XRR

By varying continuously the grazing incident angle through and few times above the critical angle for TR, the recorded XRF intensity profiles (Grazing Incidence-XRF analysis) have the potential to provide information on structural and compositional properties of thin films, such as the layer composition, sequence, thicknesses and densities, interface roughness, in depth elemental gradients of matrix elements or dopants in semiconductors, characterization of nano-particles deposited on flat surfaces, etc

A more accurate and robust reconstruction of these thin film properties requires the synergy or even the simultaneous fitting of GI-XRF with X-ray reflectometry (XRR) data



□ Total reflection X-ray Fluorescence



TXRF is essentially an energy dispersive XRF technique arranged in a special geometry.

Due to this configuration, the measured spectral background in TXRF is less than in conventional XRF. This reduction results in increased signal to noise ratio.

TXRF is a surface elemental analysis technique often used for the ultra-trace analysis of particles, residues, and impurities on smooth surfaces.



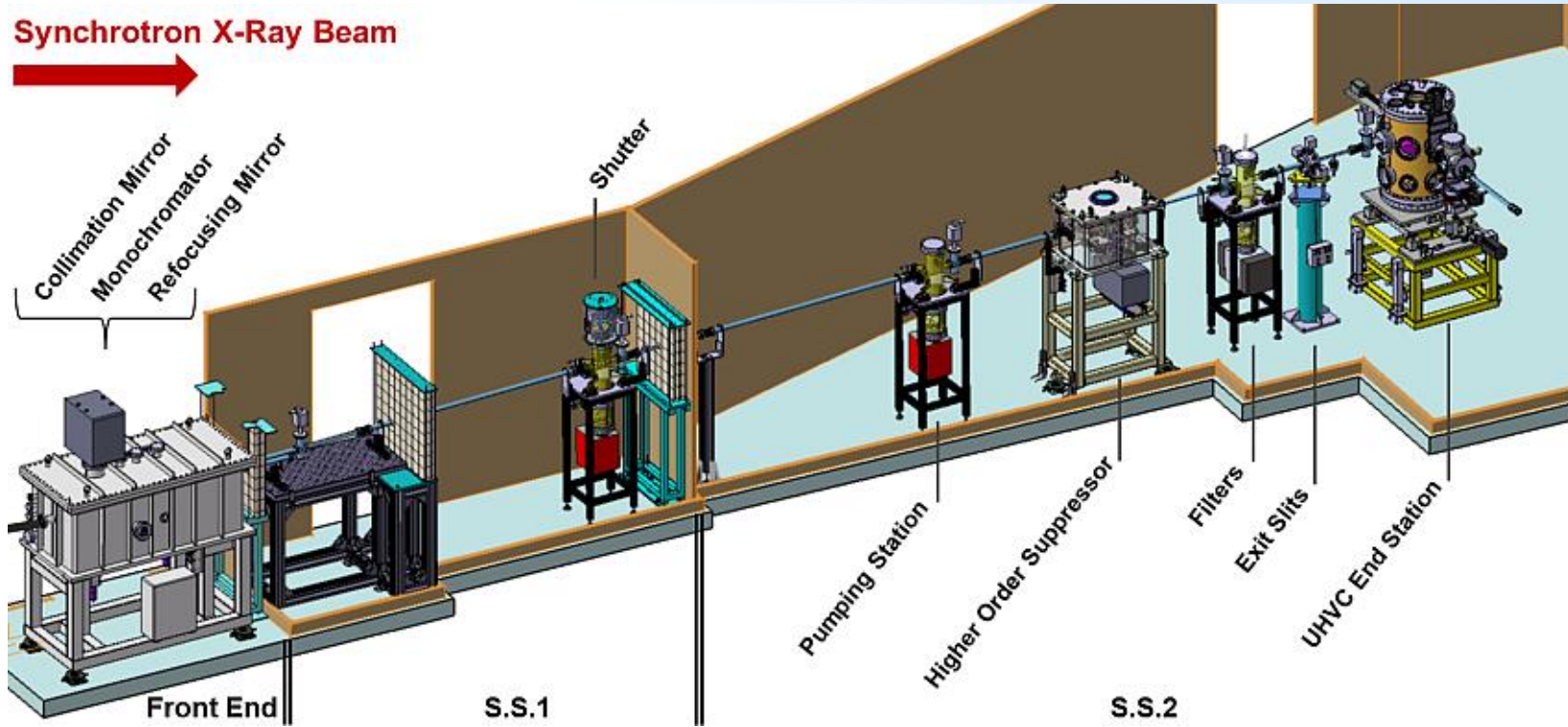
IAEA

International Atomic Energy Agency

The joint IAEA-Elettra XRF beamline at Elettra Sincrotrone Trieste



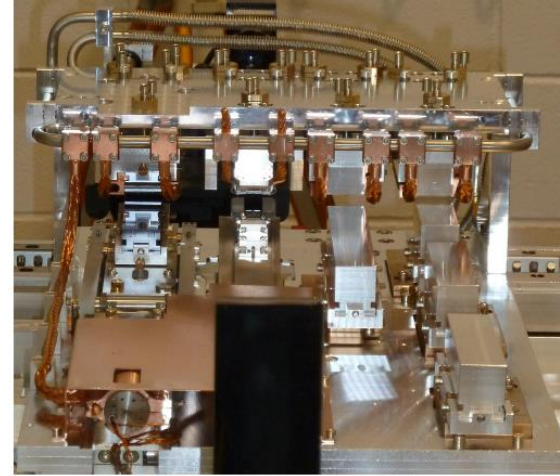
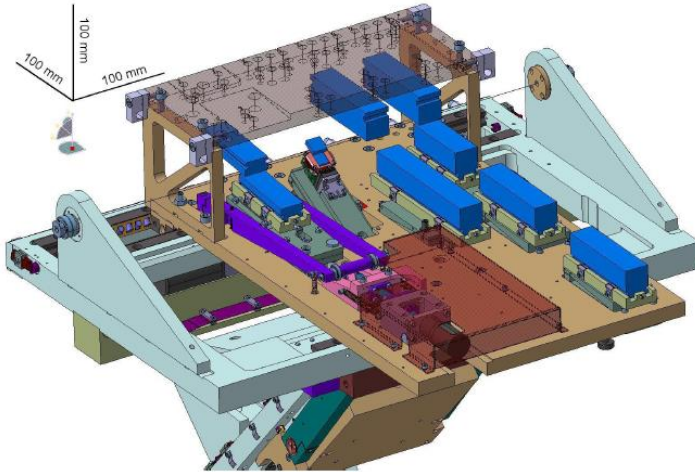
Optical layout



Source	Bending magnet
Flux	10^{10} ph/s (at 5 keV for 2.0 GeV, at 10 keV for 2.4 GeV) (Si 111)
Spot size	250 x 100 (H x V) μm^2
Beam divergence	< 0.15 mrad (at exit slits)

Werner Jark, Diane Eichert, Lars Luehl, Alessandro Gambitta, *Optimisation of a compact optical system for the beam transport at the x-ray fluorescence beamline at Elettra for experiments with small spots*, Proc. SPIE 9207, Advances in X-Ray/EUV Optics and Components IX, 92070G, 2014; doi: 10.1117/12.2063009

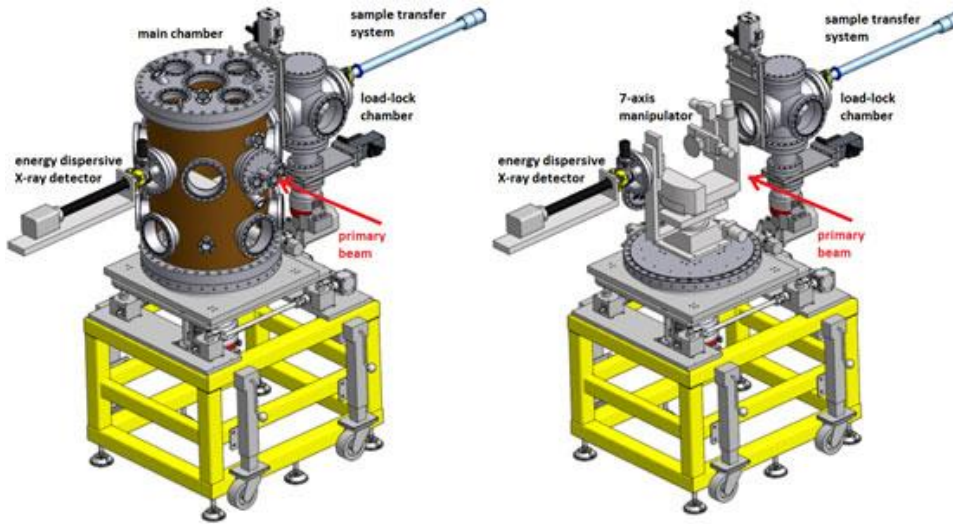
□ The monochromator at XRF



Optics type	E range (keV)	E resolution (ΔE)
Si(111)	3.6 - 14	~ 1 eV at 7 keV
InSb(111)	2.0 – 3.8	~ 1eV at 2.2 keV
ML: High E (RuB ₄ C)	4.0 – 14.0	~ 55 eV at 1 keV ~ 180 eV at 14 keV
ML: Medium E (NiC)	1.5 – 8.0	
ML: Low E (RuB ₄ C)	0.7 – 1.8	

Werner Jark *et al.*, Proc. SPIE 9207, Advances in X-Ray/EUV Optics and Components IX, 92070G, 2014; doi: 10.1117/12.2063009

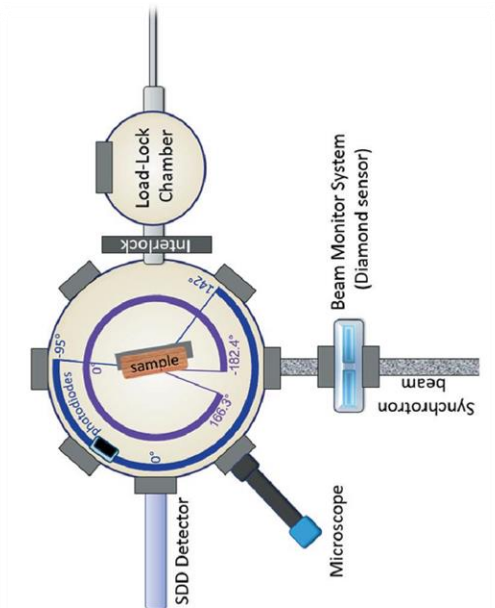
IAEXspe endstation



The IAEA end-station is based on a prototype design by Physikalisch - Technische Bundesanstalt (PTB, Berlin) and Technical University of Berlin (TUB)

Available detectors:

- Diamond detector for I_0
- SDD detector for **XRF** (different variants) and **XAS** (in fluorescence geometry)
- Photodiodes for **XAS** in transmission geometry
- Photodiodes with 100 and 200 μm slits and SDD for **XRR**



Andreas G. Karydas et al., J. Synchrotron Rad. (2018). 25, 189–203

□ 7-Axis Manipulator

Sample arm

- 3 linear stages (X, Y, Z)
- 2 goniometers (Theta, Phi)

Photodiodes arm:

- 1 linear stages (diode)
- 1 goniometer (2Theta)

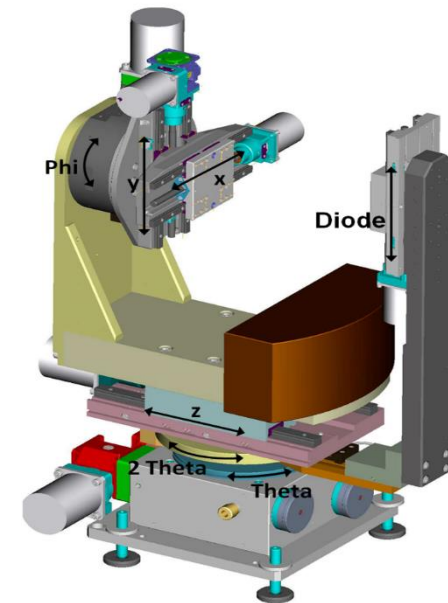
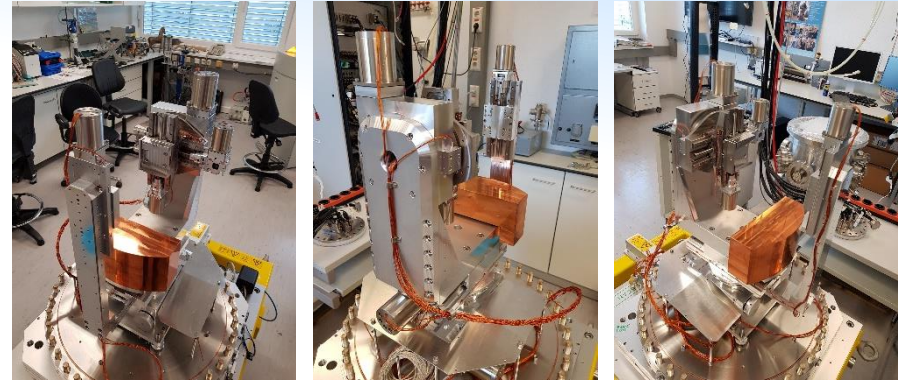
- Sample can be moved in various directions/orientations with respect to the exciting X-ray beam or with respect to the detectors.

- Ultra Thin Window (UTW) Bruker Silicon Drift detector (30 mm², FWHM 131 eV @ Mn-Ka), Si photodiodes

Full step resolution

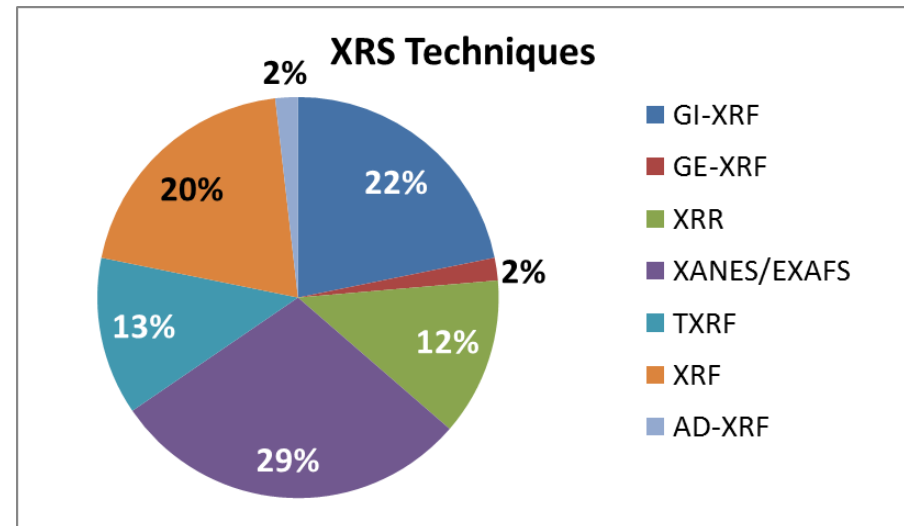
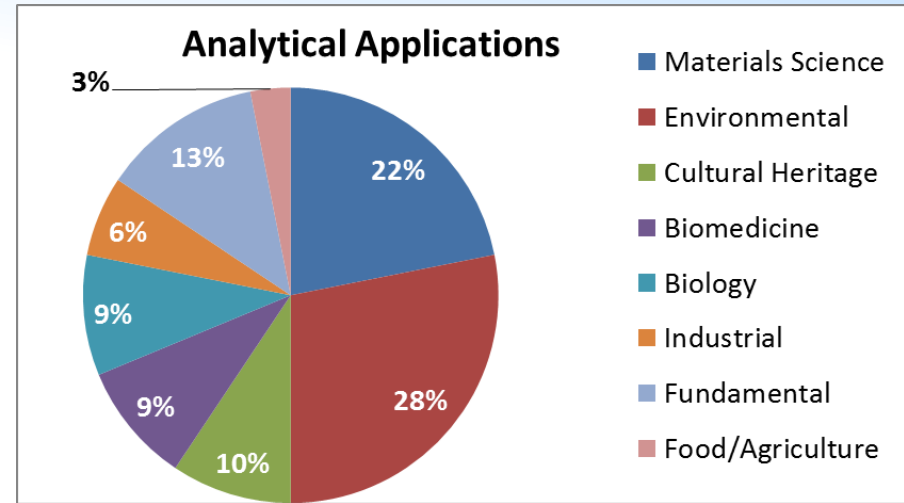
Linear axes: Diode, X, Y, Z (0.005mm, 0.005mm, 0.0005mm, 0.01mm)

Goniometers: Theta, 2theta, phi (0.001°, 0.001°, 0.005°)

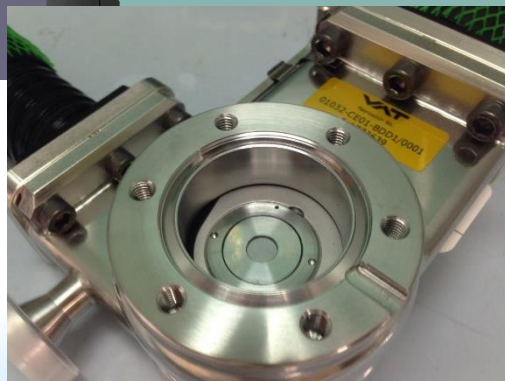
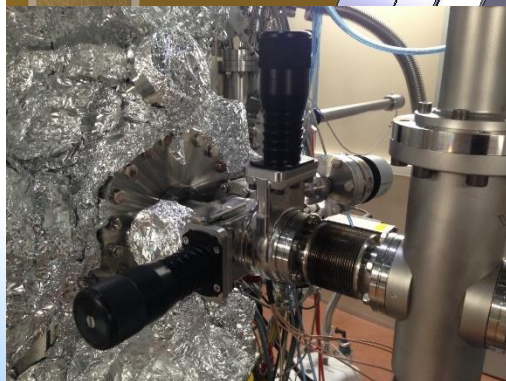
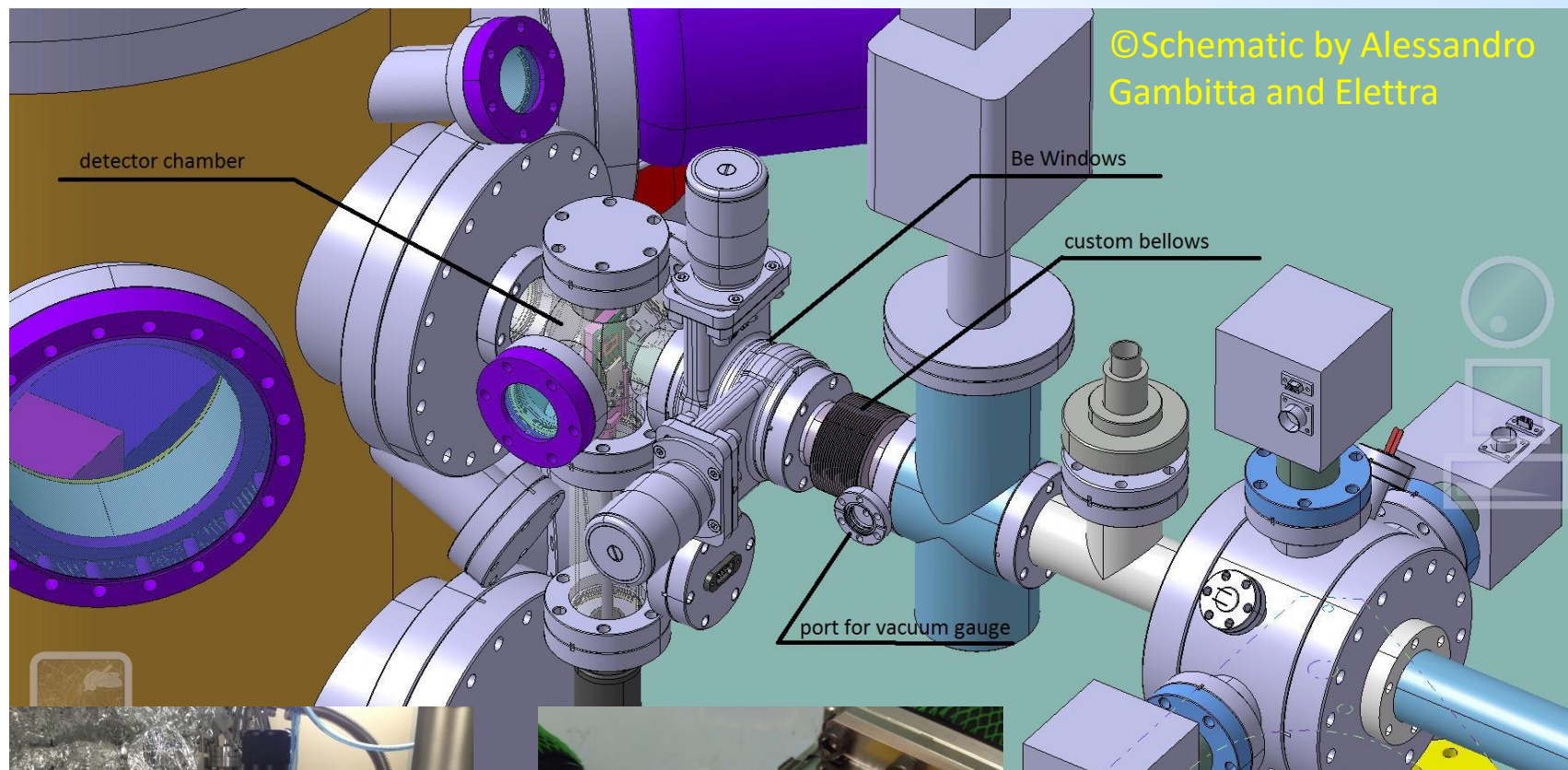


IAEA Coordinated Research Project

- **Materials Science:** Structured materials for energy storage and conversion technologies
- **Nanomedicine - Biosensing technologies**
- **Environmental monitoring** (air particulate matter, water)
- **Biological:** Elemental distribution/speciation on plant organ (leaves, roots, shoots, seeds, etc.)
- **Cultural Heritage –preventive conservation**
- **Food products security – Authenticity**
- **Determination of X-Ray Fundamental Parameters**

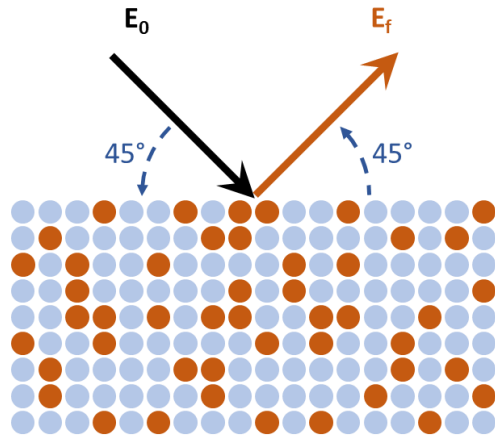


☐ non-UHV compatible samples



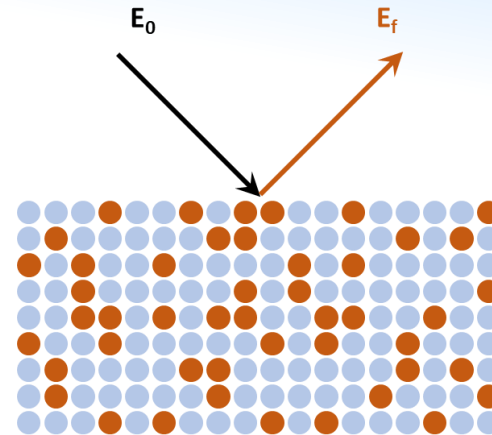
**20 μ m IF-1 Beryllium
Luxel Corporation**

Geometries and techniques



Standard 45°/45° - XRF

Elemental characterization



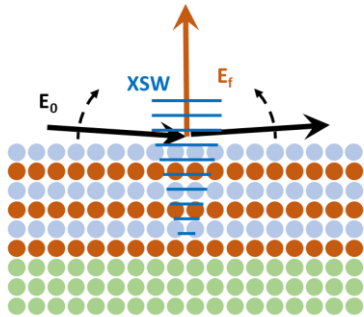
micro - XRF

Mapping

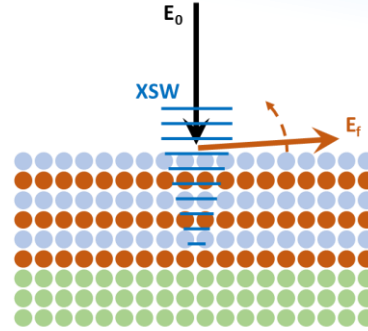


X-ray Absorption Spectroscopy
(on hot spots)

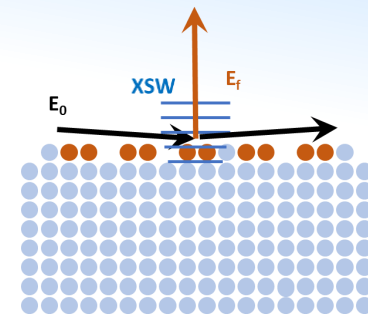
Grazing angle geometries



Grazing Incident - XRF



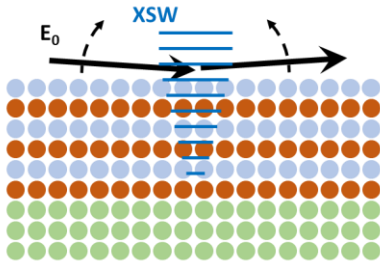
Grazing Emission - XRF



Total reflection - XRF



Depth profiling
measurements



X-Ray Reflectometry

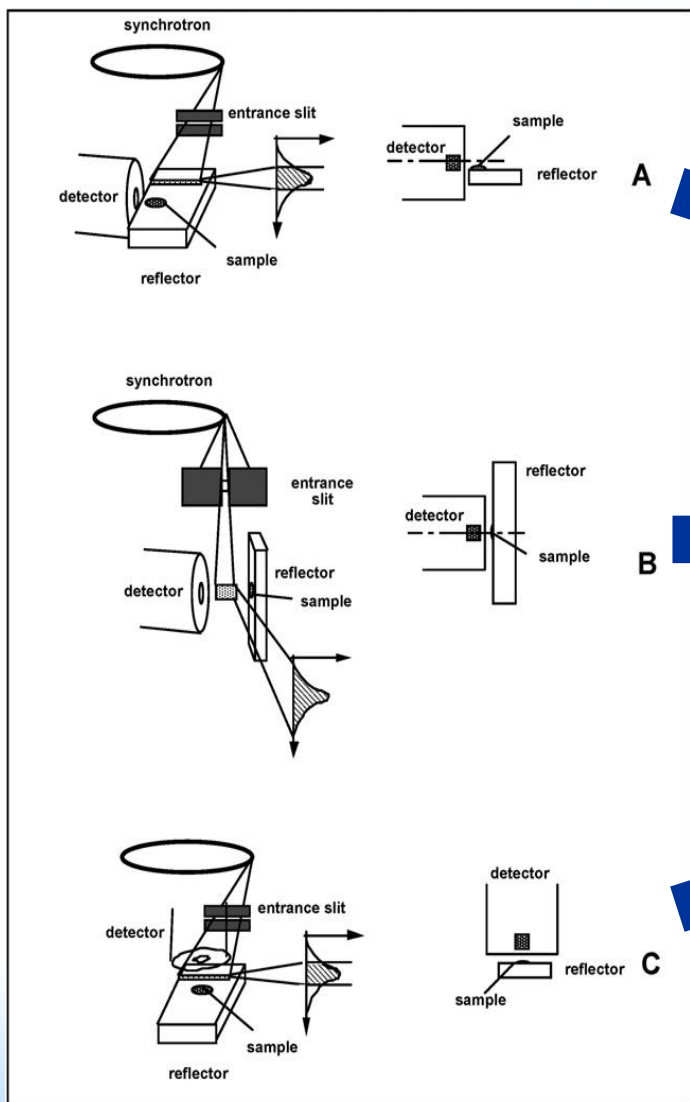
Trace element analysis
Surface contamination



X-ray Absorption Spectroscopy
(in TXRF geometry)

□ Detector geometry for TXRF

The beam is naturally vertically collimated (0.1-0.2 mrad) and has linear polarization in the orbit plane



Good excitation
No scattering
Poor detection

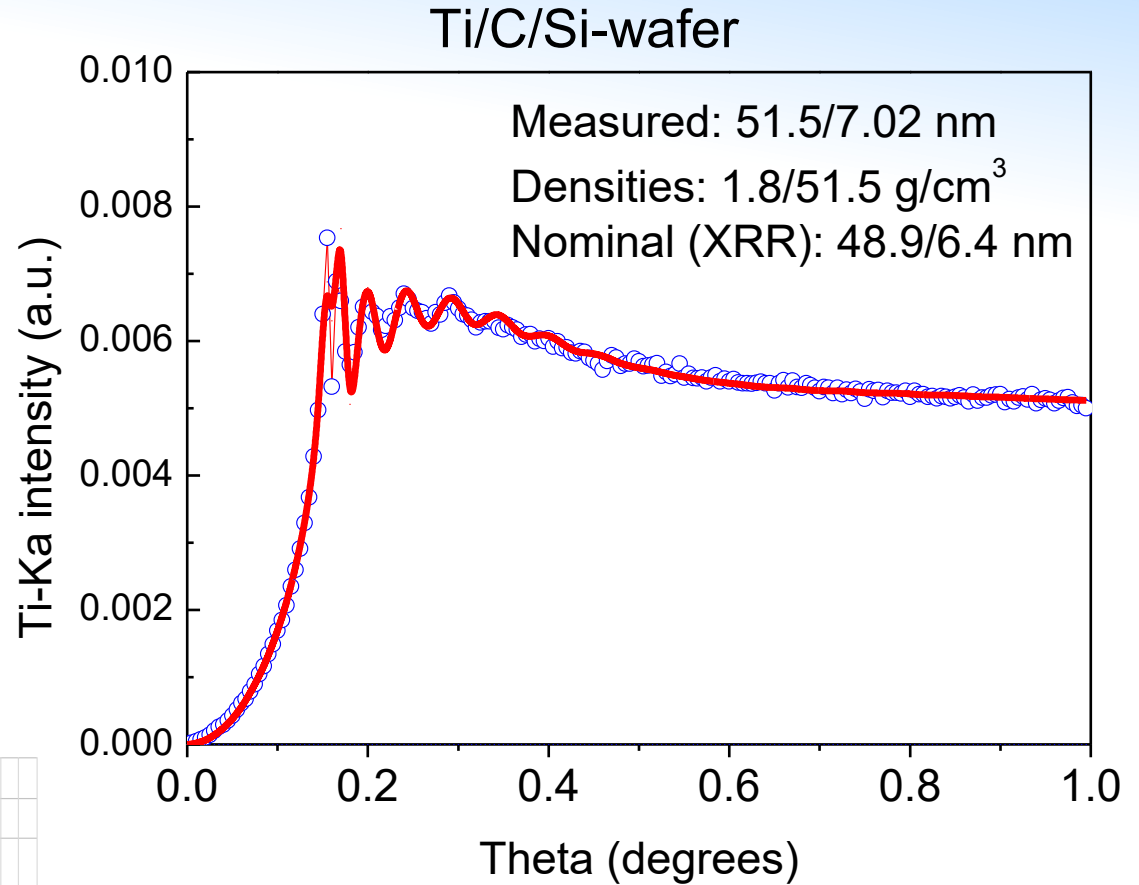
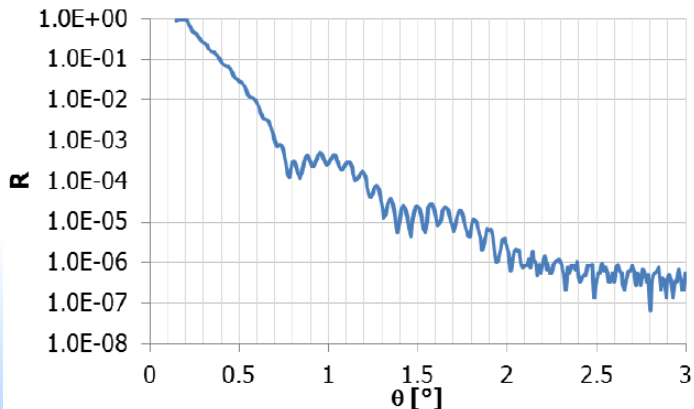
Poor excitation
No scattering
Good detection

Good excitation
Scattering
Good detection

C. Strel, P. Wobrauschek, F. Meirer and G. Pepponi,
Synchrotron radiation induced TXRF, J. Anal. At. Spectrom.,
 2008, 23, 792–798, DOI: 10.1039/b719508g

GIXRF: C/Ti double layer

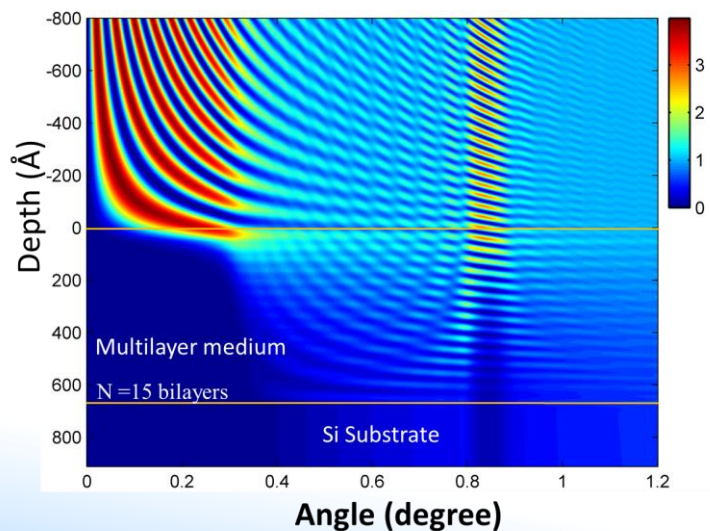
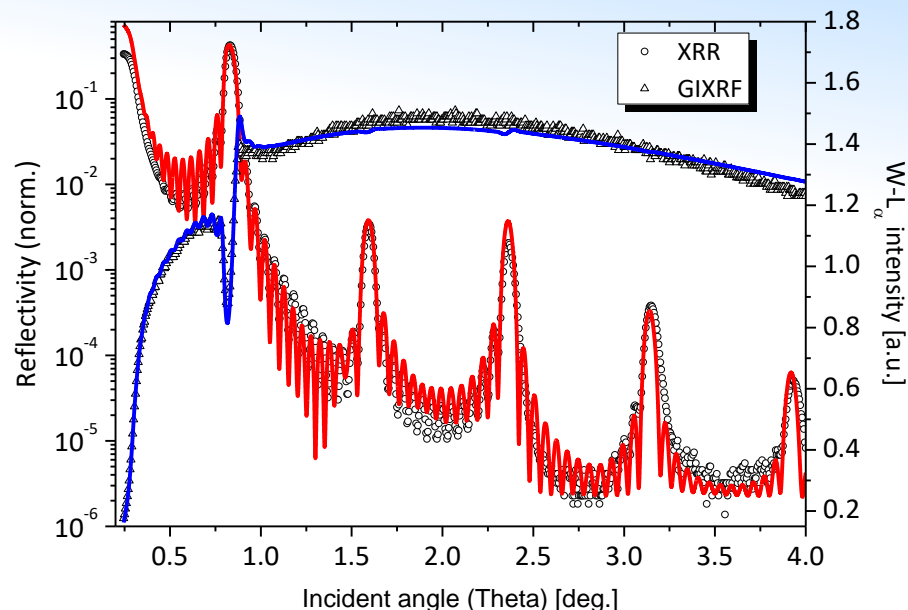
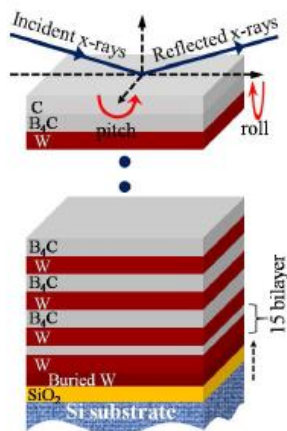
Prepared and characterized by AXO Dresden



	Fit	Nominal
Ti (nm)	7.0	6.4
C (nm)	51.5	48.9

W/B₄C multilayered (x15) thin film

Multilayered sample, prepared by the Ramanna Center for Advanced Technology, Indore, India



Electric Field Intensity (Normalized)

Layer Material	Periodicity	'B ₄ C'/'W' multilayer		
		Thickness (nm)	Roughness (nm)	Density (g/cm ³)
B ₄ C	14	1.9 ± 0.1	0.2 ± 0.1	2.10 ± 0.2
W		2.4 ± 0.2	0.3 ± 0.1	16.0 ± 0.2
B ₄ C	1	2.1 ± 0.6	0.45 ± 0.2	2.3 ± 0.2
W		3.6 ± 0.3	0.55 ± 0.2	15.5 ± 1.0
SiO ₂	1	2.0 ± 0.3	0.5 ± 0.2	2.0 ± 0.3

good agreement with previous analyses performed at the BL-16 beamline of Indus II

Zn speciation in fractionated APM

9-stage May-type cascade impactor

Sampling of size fractionated aerosol, down to 0.07 μ m size
20-3200 L of air



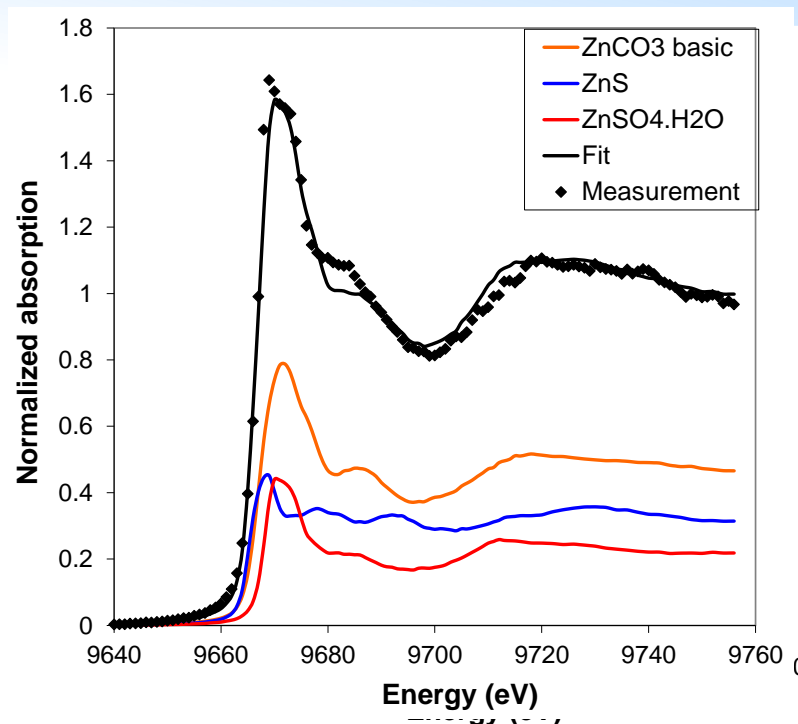
Deposited particles form a stripe of 200-500 μ m width on the 20x20 mm² Si wafer



Sample geometry well suited to SR-TXRF-XANES investigations!

J. Osan, Environmental Physics Department,
Centre for Energy Research, Budapest, Hungary

*Self-absorption correction as described in: Osán J et al., Spectrochim Acta Part B 65 (2010) 1008-1013



Sample: Paks (Hungary) 0.3 μ m, 0.6 μ m, 0.3 μ m,
Zn content: 7.39 mg/m³ (84 ng on 20 mm strip)

38% ZnSO₄, 40% ZnS, 22% Zn in glass*

Main source: Iron smelter
Burning of painted wood

Aerosols from 3D metal printing



Additive manufacturing using laser cladding

XANES: Elettra XRF and XAFS beamlines

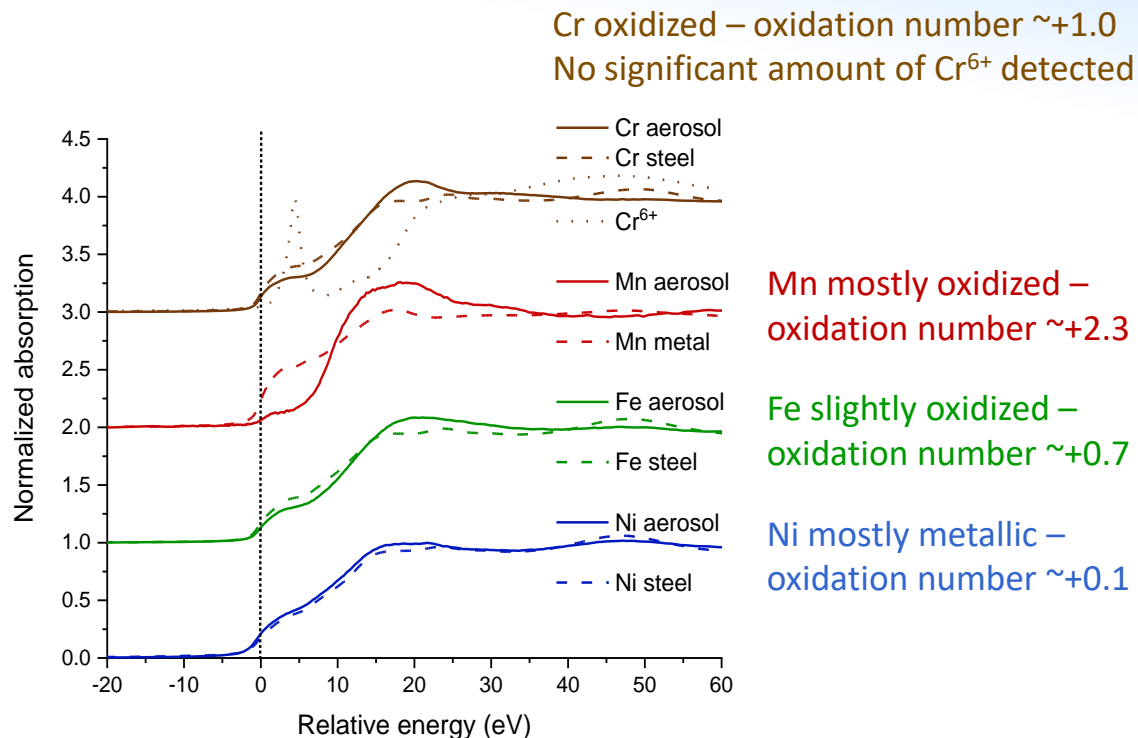


Figure courtesy: Attila Nagy, Wigner FK, Budapest, Hungary

Most of emitted aerosol particles are in the ultrafine range

Oxidation number increases with decreasing particle diameter – important for estimation of health effects

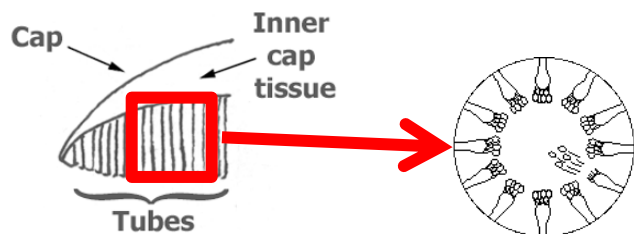
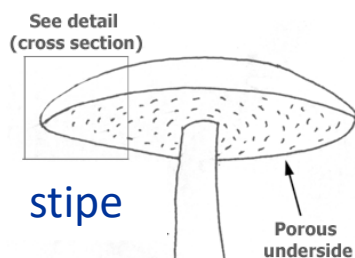
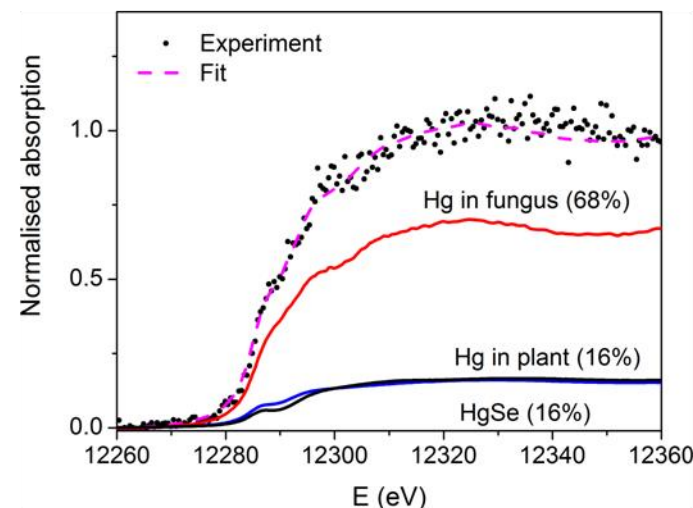
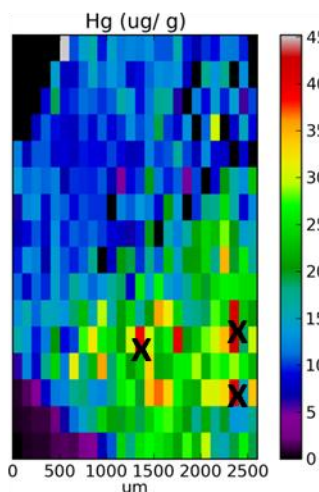
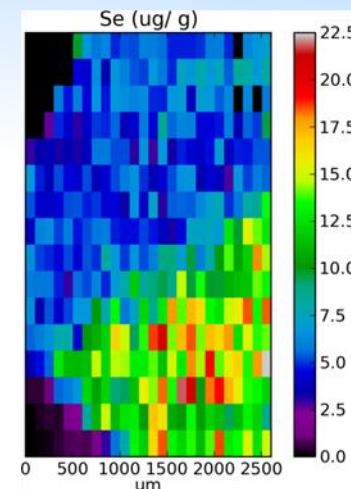
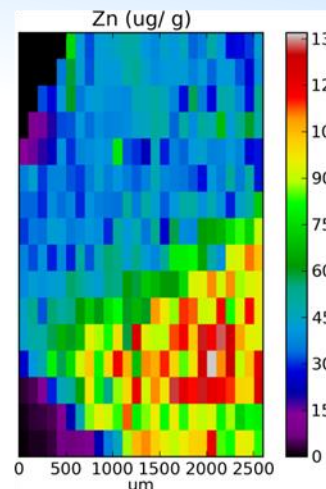
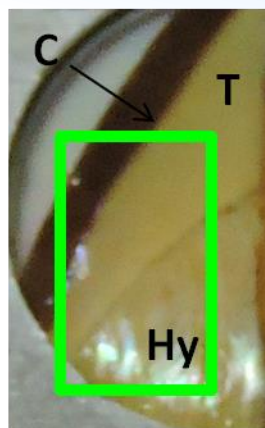
S. Kugler et al., Spectrochim. Acta Part B 2021, 177, 106110

Se and Hg in edible mushrooms

K. Vogel-Mikuš¹, P. Kump², I. Arčon³

¹ Biotechnical faculty, University of Ljubljana, ² Jozef Stefan Institute,

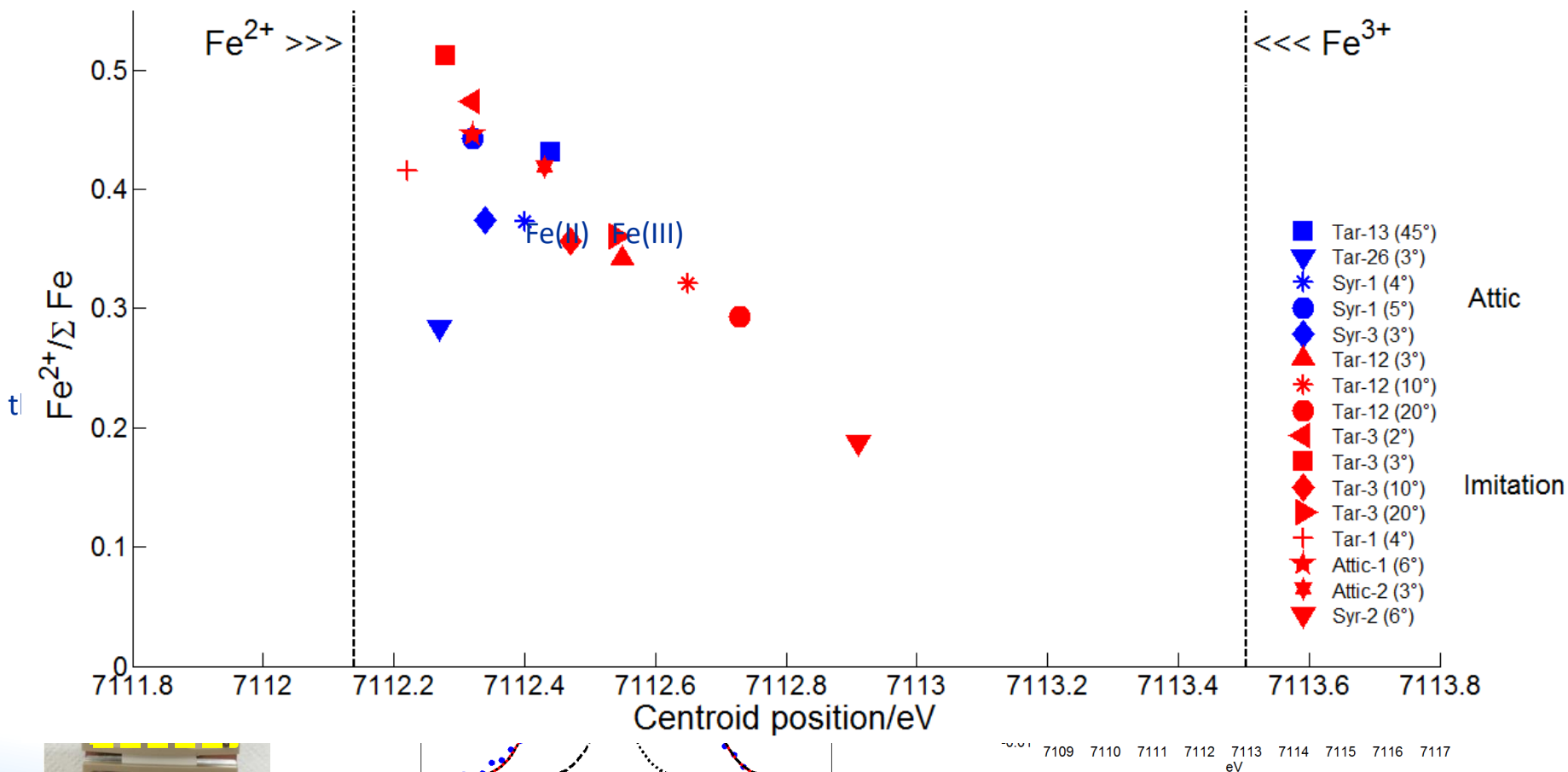
³ University of Nova Gorica



Hg is bound to tetra-cysteine proteins (metallothioneins). These proteins are digested by enzymes in the stomach and Hg is released and absorbed in our body.

GI-XANES on Black Glaze

Fe-based decorations of Ancient ceramics manufactured in South Italy



Taranto Archeological
Museum Apulo f.r.
Anonymous (Half IV
cent. b.C.)

P. Romano, C. Caliri
INFN-LNS, Catania, Italy

Analysis of gold samples

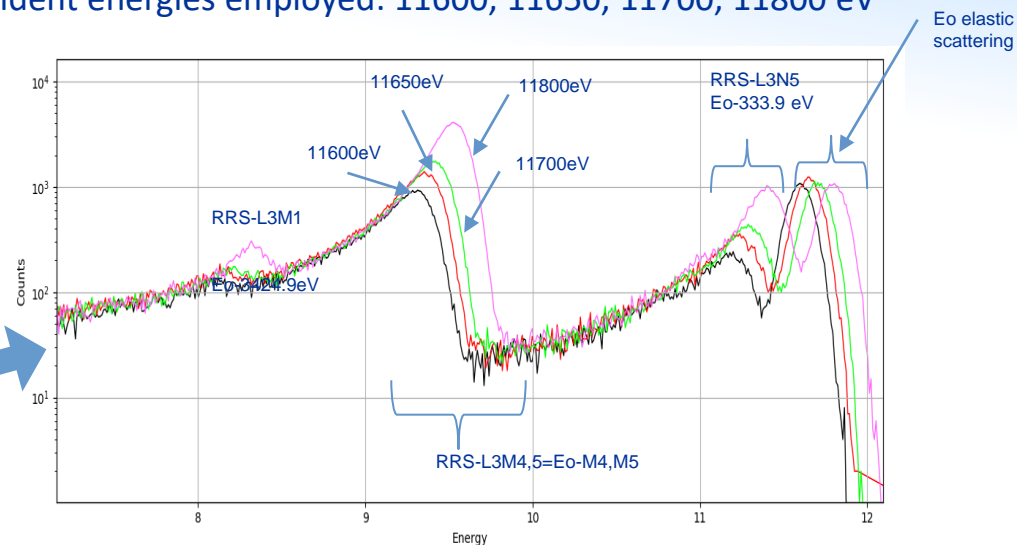
Absorption edges of Pt and Au

	Pt	Au
Z	78	79
L1 (keV)	13.88	14.353
L2 (keV)	13.273	13.734
L3 (keV)	11.564	11.919

Pt La: 9.44 keV

Synchrotron XRF spectra of pure (99.99%) thick (thickness 25 μm) gold samples

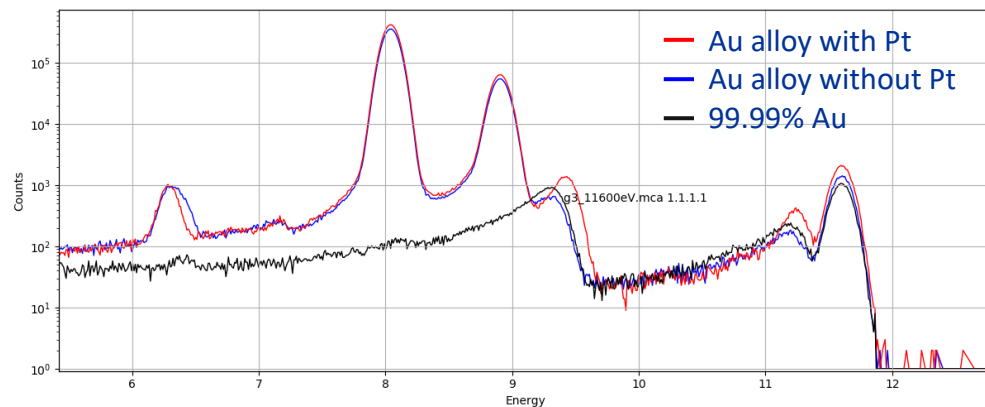
Incident energies employed: 11600, 11650, 11700, 11800 eV



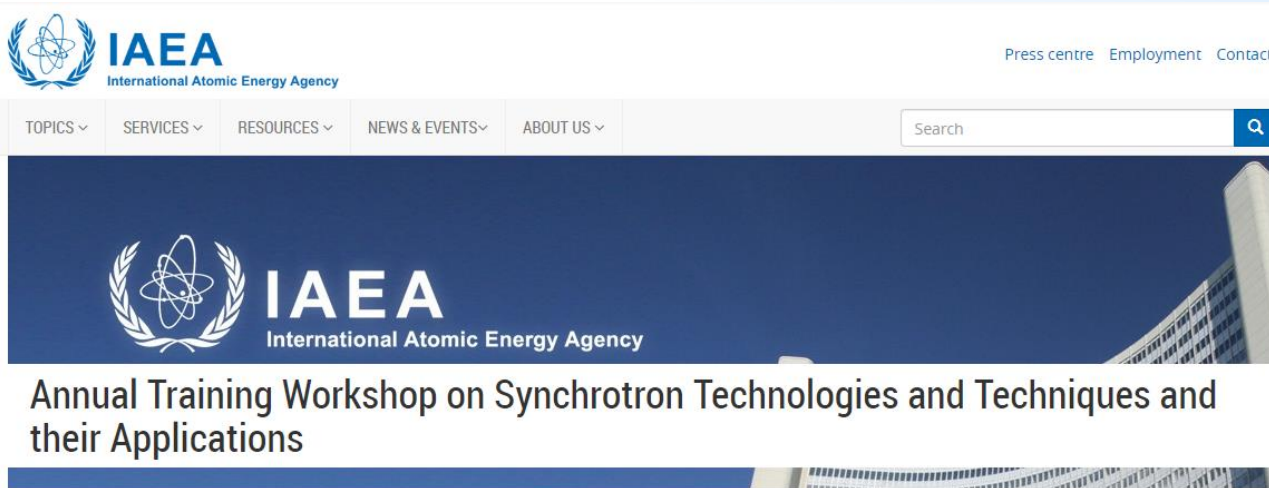
Eo=11600 eV @Elettra

Pure gold spectrum vs. Gold alloy with 0.15% Pt (Au:65.56%, Cu:25.21%, Ag:9.08%) and vs. a different certified alloy of similar composition without Pt

11600 eV > Pt(U_L3)=11564 eV



Joint IAEA-Elettra training



The screenshot shows the IAEA website header with the logo and navigation links (Press centre, Employment, Contact). Below the header is a search bar and a menu with categories: TOPICS, SERVICES, RESOURCES, NEWS & EVENTS, and ABOUT US. The main banner features the IAEA logo and the title of the event: "Annual Training Workshop on Synchrotron Technologies and Techniques and their Applications".

21 – 25 Oct 2024

Trieste, Italy

Event code:
EVT2304289

Objectives

To allow people with no or limited experience in synchrotron light experiments to participate in hands-on experiments and training at different beamlines, as well as to learn how to write successful proposal applications in order to be able to secure beamtime for themselves. The training will include experimental activities at the following beamlines operating at Elettra Sincrotrone Trieste:

- XRF
- XAFS
- MCX

Related resources

- 📄 Information Sheet
- 📄 Participation Form (Form A)
- 📄 Grant Application Form (Form C)

The next training **will be announced soon** and will be held in the period **26-30 May 2025**

SISSI beamline (FTIR microscopy) will replace MCX beamline (X-ray diffraction)



IAEA

International Atomic Energy Agency

Thanks for your attention!

Alessandro Migliori

a.migliori@iaea.org

<https://nucleus-new.iaea.org/sites/nuclear-instrumentation/Pages/Home.aspx>

<https://www.elettra.trieste.it/lightsources/elettra/elettra-beamlines/microfluorescence/x-ray-fluorescence.html>